1-1-2020

Alkali-Metal Sulfide as Cathodes toward Safe and High-Capacity Metal (M = Li, Na, K) Sulfur Batteries

Huiling Yang
University of Wollongong, hy978@uowmail.edu.au

Binwei Zhang
University of Wollongong, binwei@uow.edu.au

Yunxiao Wang
University of Wollongong, yunxiao@uow.edu.au

Konstantin K. Konstantinov
University of Wollongong, konstan@uow.edu.au

Hua-Kun Liu
University of Wollongong, hua@uow.edu.au

See next page for additional authors

Alkali-Metal Sulfide as Cathodes toward Safe and High-Capacity Metal (M = Li, Na, K) Sulfur Batteries

Abstract

© 2020 Wiley-VCH GmbH Rechargeable alkali-metal–sulfur (M–S) batteries, because of their high energy density and low cost, have been recognized as one of the most promising next-generation energy storage technologies. Nevertheless, the dissolution of metal polysulfides in organic liquid electrolytes and safety issues related to the metal anodes are greatly hindering the development of the M–S batteries. Alkali-metal sulfides (M2Sx) are emerging as cathode materials, which can pair with various safe nonalkali-metal anodes, such as silicon and tin. As a result, the combined M2Sx cathode-based M–S batteries can achieve high capacity as well as safety, thereby providing a more feasible battery technology for practical applications. In this review, recent progress in developing M2Sx cathode-based M–S batteries is systematically summarized, including the activation methods for M2Sx cathodes, M2Sx cathode optimization, and the improvement of electrolytes and anode materials. Furthermore, perspectives and future research directions of M2Sx cathode-based M–S batteries are proposed.

Disciplines

Engineering | Physical Sciences and Mathematics

Publication Details

Yang, H., Zhang, B., Wang, Y., Konstantinov, K., Liu, H. & Dou, S. (2020). Alkali-Metal Sulfide as Cathodes toward Safe and High-Capacity Metal (M = Li, Na, K) Sulfur Batteries. Advanced Energy Materials,

Authors

Huiling Yang, Binwei Zhang, Yunxiao Wang, Konstantin K. Konstantinov, Hua-Kun Liu, and Shi Xue Dou

DOI: 10.1002/ ((please add manuscript number))

Article type: Review

Alkali-metal sulfide as cathodes towards safe and high-capacity metal (M = Li, Na, K) sulfur batteries

Hui-Ling Yang, Bin-Wei Zhang, Yun-Xiao Wang, Konstantin Konstantinov, Hua-Kun Liu* and Shi-Xue Dou*

H. Yang, Dr. B. Zhang, Dr. Y. X. Wang, Prof. K. Konstantinov, Prof. H.K. Liu and Prof. S. X. Dou

Institute for Superconducting and Electronic Materials, Australian Institute of Innovative Materials, University of Wollongong, Innovation Campus, Squires Way, North Wollongong, New South Wales 2500, Australia.

E-mail: yunxiao@uow.edu.au; hua@uow.edu.au

Keywords: metal–sulfur batteries, alkali-metal sulfide cathodes, electrolytes, anodes

Rechargeable alkali-metal–sulfur (M–S) batteries, because of their high energy density and low cost, have been recognized as one of the most promising next-generation energy storage technologies. Nevertheless, the dissolution of metal polysulfides in organic liquid electrolytes and safety issues related to the metal anodes are greatly hindering the development of the M–S batteries. Alkali-metal sulfides (M_2S_x) are a emerging as cathode material, which can pair with various safe nonalkali-metal anodes, such as silicon and tin. As a result, the combined M_2S_x cathode-based M–S batteries could achieve high capacity as well as safety, thereby providing a more feasible battery technology for practical applications. In this review, recent progress in developing M_2S_x cathode-based M–S batteries will be systematically summarized, including the activation methods for M_2S_x cathodes, M_2S_x cathode optimization, and the

improvement of electrolytes and anode materials. Furthermore, perspectives and future research directions of M_2S_x cathode-based M–S batteries will be proposed.

1. Introduction

Despite the established products in portable electronic devices, conventional lithium ion batteries (LIBs) are insufficient for the development of newly emerging markets, such as the key markets for electric vehicles or hybrid vehicles, so there is an urgent demand for further developments in energy density and safety.[1,2] Currently, the commercial LIBs with transition metal oxide/phosphate cathodes such as $LiCoO_2$, $LiMn_2O_4$, and $LiFePO_4$ are close to their limited theoretical energy density. A very promising approach to solve this problem is to move from the traditional insertion chemistry to an innovative conversion chemistry.[3-5] The alkali lithium–sulfur (Li–S) system is a good example of this, since the sulfur cathode could deliver a high theoretical capacity of 1675 mA h g^{-1} based on the following electrochemical process: $16Li + S_8 \rightarrow 8Li_2S$, offering an extraordinarily higher specific energy density than that provided by conventional LIBs, i.e. 2,600 W h kg^{-1} *vs.* 300 W h kg^{-1}.[6-8] In addition, sulfur is abundant on earth, and also very low-cost and environmentally benign. Similarly, the practical development of various alkali-metal–sulfur (M–S, M = Li, Na, and K) batteries has been hindered by a series of issues, which include: i) the polysulfide shuttle effect, which causes low capacity with limited cycle life[9,10]; ii) the high reactivity of the alkali metal anodes, which presents safety issues,[11-13] and iii) the poor electronic conductivity of the sulfur cathode materials, which leads to low sulfur utilization and poor rate capability.[14,15]

To address the above technical challenges for metal–sulfur batteries with sulfur powder-based electrodes, alternative solutions for the architectural design of sulfur electrodes must be pursued. Therefore, the development of discharged sulfur electrodes, indeed

alkali-metal sulfide (M_2S_x) cathodes, has become very interesting and imperative. Compared to the mechanical disadvantage of sulfur powder-based cathodes, M_2S_x cathodes do not suffer from volume collapse, since their volume shrinkage during the initial charge process could generate enough space to accommodate the following volume expansion of sulfur during the discharge process, leading to more stable cycling performance for the M–S batteries.[16] In addition, as the metallized sulfur, M_2S_x cathodes have a huge natural advantage, in that they can be coupled with alkali metal-free anodes such as graphite or silicon (Si). Consequently, the fatal short-circuiting caused by the excessive growth of dendrites on alkali metal anodes could be greatly adverted, creating safer and more stable M–S batteries.[17, 18] Besides, the M_2S_x cathodes hold great promise for high energy battery system. For instance, Li_2S has a high specific capacity of 1166 mA h g^{-1}.[19] When coupled with Si anodes, Li_2S-based Li–S batteries can deliver a high specific energy, which is four times of the $LiCoO_2$/graphite system.[20] Therefore, the M_2S_x cathode-based M–S batteries could be applied as safe, cost-effective, high durable battery technology with comparatively high energy densities.

Unfortunately, it is challenging to apply M_2S_x cathodes, which usually show high initial charge potential due to their high electronic resistivity and low ion diffusivity.[20] The low electronic and ionic conductivity of the M_2S_x cathodes also leads to low sulfur utilization and poor rate capability.[21] Moreover, the widely used ether-based electrolytes in M–S batteries could be decomposed at high potential, resulting in deteriorating electrochemical performance of the M_2S_x-based M–S batteries.[22] Some efforts have been made to reduce the initial activation barrier of M_2S_x in recent years. Reducing the M_2S_x particle size is one effective approach to improve the electrode kinetics, hence reducing its initial charging over-potential. Furthermore, from sharing the analogous conversion mechanisms with the sulfur cathodes, M_2S_x cathodes possess

similar problems, with the most severe one the "shuttle effect", which leads to the low Coulombic efficiency (CE) and shortened cycle life of M–S batteries. Promising methods for boosting the electrochemical performances of the M_2S_x cathodes are similar to those for the S_8 cathodes, including minimizing size of the M_2S_x nanoparticles,[23-25] integrating M_2S_x with carbonaceous frameworks,[26-29] applying polar host materials with fabulous polysulfide intermediate absorptivity,[30,31] and using electrolyte additives or creating new electrolyte systems.[32] These strategies have greatly enhanced the electrochemical performance of the M_2S_x-based half-cells. Most of these approaches, however, still suffer from the unavoidable shuttling effect, which limits the further application of M_2S_x cathodes in the fabrication of full-cells with non-Li/Na/K anodes.[33] In this review, we summarize the electrochemical mechanism of M_2S_x cathode-based M–S batteries, and discussed different strategies to lower the overpotential barrier of M_2S_x, which is significant for the activation of M_2S_x cathodes, as schematically depicted in **Figure 1**. In addition, the M_2S_x electrode design, including the synthesis and the components of M_2S_x cathodes are discussed. Moreover, commonly used electrolytes and additives, especially all-solid-state electrolytes, and the potential for the application of "full-cell" batteries, are reviewed in detail.

2. Principles of alkali-metal sulfide as cathodes

Table 1 summarizes the thermodynamically stable phases within the binary systems of Li–S, Na–S, and K–S at room temperature (RT). According to the previous study on Li–S phase diagram, Li_2S is the only thermodynamically stable binary Li–S phase.[34] Unlike the immiscibility of S-rich liquid phase in the Li–S system, the Na–S and K–S phase diagrams[35] display a series of stable phases of Na_2S_x (x = 1, 2, 4, and 5) and K_2S_x (x = 1, 2, 3, 4, 5, and 6) at room temperature, respectively.[36-38]

Taking the Li– and Na–S systems as examples, **Figure 2** illustrates the components of the conventional M–S batteries and M_2S_x cathode-based M–S batteries, respectively. It is evident that both battery systems show the typical shuttle effect due to the formation of polysulfide species. The conventional M–S batteries consist of a metal anode and an S cathode; the ideal reaction during the discharge/charge process would be: $2M + 1/8\ S_8 \rightleftarrows M_2S$ (M = Li or Na). The full reduction of sulfur from S to S^{2-} possesses a capacity of 1672 mA h g_s^{-1}.[39] The utilization of metal anode is very problematic, however, because it is prone to show an unstable solid-electrolyte interphase (SEI), unlimited volume change, and fatal dendrite growth, thus leading to inferior battery performance and safety issues. By contrast, for the M_2S_x cathode-based M–S batteries, the cathode is replaced by Li-/Na-containing sulfides; the selection of the anodes is very flexible compared with traditional anodes that are utilized in Li-/Na-ion batteries. The specific reaction mechanisms will be discussed separately below. Significantly, due to the utilization of non-alkali-metal anodes, such as silicon or tin, the safety concerns can be completely overcome, with enhanced battery performance.

2.1 Principles of Li_2S-based Li–S batteries

Li_2S was considered to be electrochemically inactive due to its electronically and ionically insulating properties.[40] To date, various efforts have been made to activate Li_2S. Based on the previously reported research,[20, 41] the Li_2S cathode needs to overcome the energy barrier at the beginning of the charging process. It is well-known that the energy barrier of commercial Li_2S cathode material is above 3.5 V.[33] Three kinetic factors, electronic conductivity of Li_2S, diffusivity of the Li^+ in Li_2S, and charge transfer at the surface of Li_2S, influence the magnitude of the potential barrier.[42] When the outer surface layer of Li_2S is oxidized into lithium polysulfides (Li_2S_x, $4 \leq x \leq 8$), the energy barrier will disappear. This phenomenon is attributed

to the fact that the lithium bonding energies of Li_2S and lithium polysulfides are close, which enables free charge transfer between Li_2S and the lithium polysulfides.[20] In addition, the lithium polysulfides could act as nucleation centres in the electrolyte, resulting in a deficiency of Li^+, and then it will cause immediate phase separation of the surface of Li_2S. Thus, the charge transfer process could be easier in the electrolyte. Consequently, a little overpotential can be observed after the initial activation during the first charging cycle. The voltage window of Li_2S-based Li–S batteries after the initial charge process is similar with that of sulfur based Li–S batteries, which is 1.8-2.8 V *vs.* Li/Li^+.

Specifically, as shown in **Figure 3**a, the initial charging state can be divided into four stages.

Stage I: the Li_2S will first release Li^+ and electrons, and then generate the solid $Li_{2-x}S$ before the cut-off voltage is reached:

$$Li_2S(s) \rightarrow Li_{2-x}S(s) + xLi^+ + xe^- \quad (1)$$

Core/shell structured $Li_2S@Li_{2-x}S$ is generated as illustrated in Figure 3 (Step 2), with a high deficiency of Li^+ in the $Li_{2-x}S$ surface layer. It is a slow charge transfer process, which will result in a high charge-transfer resistance (large potential barrier).

Stage II: With further charging of Li_2S, polysulfides will be generated:

$$y\ Li_2S(s) \rightarrow Li_2S_y(l) + (2y - 2)\ Li^+ + (2y - 2)\ e^- \quad (2)$$

Stage III: The soluble Li_2S_y is converted into the Li_2S_8 phase:

$$Li_2S_y(l) \rightarrow y/8\ Li_2S_8(l) + (2 - y/4)\ Li^+ + (2 - y/4)\ e^- \quad (3)$$

Stage IV: The soluble Li_2S_8 phase is transformed into elemental sulfur:

$$8Li_2S_8(l) \rightarrow S_8(s) + 2Li^+ + 2e^- \quad (4)$$

To directly detect the exact oxidation mechanism of Li_2S, Kim et al.[43] used a special double-layer separator cell to isolate Li_2S particles from the carbon cathode (Figure 3b). Interestingly, the Li_2S particles still deliver a considerable capacity during the initial charge and discharge process, the results indicate that the electrochemical oxidation of Li_2S occurs not only through

a direct charge transfer between solid Li_2S and conducting materials but through chemical reactions coupled with the charge transfer process. They proposed reaction mechanism was based on the existence of soluble polysulfides impurities accompanied with Li_2S particles. These soluble polysulfides (S_n^{2-}, $n \leq 4$) are firstly oxidized to long chain polysulfides (n = 6, 8), then react with Li_2S to generate medium chain polysulfides. The chemical reactions can be expressed as:

$$S^{2-}\,(s) + S_n^{2-}\,(l,\ n = 6, 8) \rightarrow S_k^{2-}\,(l) + S_{n-k+1}^{2-}\,(l) \qquad (5)$$

2.2. Principles of Na_2S-based RT Na–S batteries

Among stable phases of Na_2S_x (x = 1, 2, 4, and 5), the present research is focused on Na_2S due to its having the highest theoretical capacity (686 mA h g^{-1}). According to its electrochemical performance and the corresponding characterizations, the reactions during the initial charge process for Na_2S cathode can be expressed as[44]:

$$n Na_2S \rightarrow Na_2S_n\ (4 \leq n \leq 8) + (2n\text{-}2)\ Na^+ + (2n\text{-}2)\ e^- \qquad (6)$$

$$Na_2S_n\ (4 \leq n \leq 8) + (2n\text{-}2)\ Na^+ + (2n\text{-}2)\ e^- \rightarrow nS + 2nNa^+ + 2ne^- \qquad (7)$$

Similar to the Li_2S cathode, the Na_2S cathode encounters a potential barrier for the phase-nucleation of sodium polysulfides as well, which is ascribed to the facts that the Na_2S also has high electronic resistivity and low sodium ion diffusivity. The voltage window for Na_2S cathode based RT-Na–S batteries is up to 3.0 V, compared to that of sulfur cathode. (2.8 V vs. Na/Na^+) **Figure 4**a shows the charge-discharge profiles of the first two cycles of a room-temperature Na–S (RT-Na–S) battery, and the corresponding cyclic voltammetry (CV) results are displayed in Figure 4b. It is clear that the activation process for Na_2S is much harder than that for Li_2S during the first charge.

2.3. Principles of K_2S_x-based RT K-S batteries

Although RT K−S battery delivers lower theoretical energy density (914 W h kg_{K2S}^{-1}) than Li/Na−S batteries due to the lower discharge voltage (1.88 V) and higher atomic weight of K, it has distinctive advantages of high elemental abundance (both K and S) and low standard reduction potential of −2.93 V(K^+/K vs. standard hydrogen redox potential) than that of Na^+/Na (−2.71 V).[45] The first report on RT potassium–sulfur batteries was in 2014,[11] but the electrochemical reaction mechanism on the sulfur cathode is still not fully understood. The K–S phase diagram, including a series of stable phases of K_2S_x (x = 1, 2, 3, 4, 5, and 6), provides a new direction to study the mechanism of K–S batteries by applying pure-phase polysulfides.[46] Unlike lithium and sodium polysulfides, the short-chained K_2S_x ($x \leq 4$) cannot dissolve in the ether-base electrolytes, such as diethylene glycol dimethyl ether (DEGDME). According to the previous studies on RT K–S batteries, there is a K_2S "dead" sulfur species, which are not able to be charged during cycling; K_2S_3 was usually detected as the major final discharge product in K–S batteries.[11,47] This was further confirmed by the research on K_2S cathode. The voltage window for K_2S_x cathode based RT-K–S batteries is 1.2–3 V, corresponding with that of sulfur based K–S batteries. **Figure 5**a shows that K_2S showed no oxidation or reduction current during the galvanostatic cycling test, indicating that K_2S cannot form polysulfides without any contribution to reversible capacity. Wu et al.[48] synthesized K_2S_2 and K_2S_3, and investigated their mechanism. The double-layer separator cell delivers notable lower discharge capacity for both K_2S_3 and K_2S_2 cathodes, while the charge curves and capacities are similar in both the single- and double-separator cells, indicating the further discharge of K_2S_3 is dominated by the solid reaction and the solution pathway contributes mostly to the charge capacity. The reaction mechanism during the initial cycle can be verified from the experiments (Figure 5b).

Discharge:

Electrochemical reactions:

$$2K_2S_3(s) \rightarrow 3K_2S_2(s) + 2e^- - 2K^+ \quad (8)$$

$$2K_2S_3(s) \rightarrow 3K_2S(s) + 4e^- - 4K^+ \quad (9)$$

$$K_2S(s) \rightarrow 2K_2S(s) + 2e^- - 2K^+ \quad (10)$$

Charge:

Chemical reactions:

$$3K_2S_x\ (x = 2, 3) \rightarrow (4-x)\ K_2S + 2(x-1)\ K^+ + (x-1)\ S_4^{2-} \quad (11)$$

$$(4-x)\ S_6^{2-} + 2K_2S_x(s)\ (x = 1, 2, 3) \rightarrow (6-x)\ S_4^{2-} + 4K^+ \quad (12)$$

Electrochemical reactions:

$$3S_4^{2-} \rightarrow 2S_6^{2-} + 2e^- \quad (13)$$

$$2S_4^{2-} \rightarrow S_8 + 2e^- \quad (14)$$

The discharge overpotential in this system are as high as 0.8 V even under low current density (20 mA g^{-1}), indicating a kinetically sluggish reduction reaction for involving insulated solid-phase products like K_2S_3, K_2S_2, and K_2S. The charging process involving soluble phase reactions requires much lower overpotential, due to its fast kinetics. However, K_2S cannot be charged, given the assumption that a possible way to reducing the capacity decay of K−S batteries by minimizing the formation of K_2S.

To study the mechanism of solution-phase K_2S_n ($5 \leq n \leq 6$) catholyte, Sun et al.[49] loaded it into a carbonaceous framework of three-dimensional freestanding carbon nanotube (3D–FCN). The initial discharge-charge curves of the K|K_2S_n catholyte|FCN half-cell and the K impregnated HC| K_2S_n catholyte|FCN full-cell are displayed in Figure 5c, and the electrochemical reaction in the catholyte is:

$$S_n^{2-}\ (5 \le n \le 6) \xrightarrow{discharge} K_2S_3 \xrightarrow{charge} S_5^{2-} \qquad (15)$$

Since K_2S_3 is formed *in-situ* from polysulfide nuclei in the electrolyte after the first discharge, it significantly improves the charge transfer in the following cycles, so that there is no obvious overpotential for the following charging process.

3. Activation processes

Due to the intrinsic electronic insulating properties and insoluble nature of M_2S_x-based cathodes, they feature high charge transfer resistance during the first charge process,[20] so that they require an initial activation at high potential (up to 4 V) to overcome the thermodynamic and kinetic barriers. As a result, various approaches have been proposed to reduce the high activation overpotential of M_2S_x as well as to limit the irreversible diffusion of polysulfides. The following methods are expected to promote the electrochemical performance of the M_2S_x-based M-S batteries:

3.1. Reducing the size of M_2S_x particles

Refined M_2S_x particles with high surface area can increase the ionic conductivity of M_2S_x cathode and shorten ionic/electronic migration distances. They can significantly speed up the kinetic process of M_2S_x oxidation.[20] Two typical approaches, including ball milling of commercial Li_2S particles and heat treatment of Li_2SO_4, have been developed to reduce the particle size and the activation voltage of Li_2S.[50-52] As Li_2S is sensitive to air and moisture, however, the ball milling process requires harsh experimental conditions. It is more practical to reduce Li_2SO_4 or form Li_2S *in-situ* from other sulfur sources. Wolden et al.[53] developed an alternative approach by reacting hydrogen sulfide (H_2S) with a metal-organic solution for scalable synthesis of Li_2S nanocrystals. The prepared cathodes yielded 98.5% of their theoretical capacity as well

as promising cyclability and rate capability. Wang et al.[54] also showed that re-precipitated Na_2S nanospheres with smaller size had higher electrochemical reactivity.

3.2. Adding conductive carbon

The incorporation of a conductive carbon framework is also very critical to reduce the overpotential of M_2S_x cathodes. Carbon can enhance the conductivity of the M_2S_x cathodes, and the high surface area of carbon could also simultaneously accommodate the formation of M_2S_x. Carbon materials ranging from one-dimensional (1D) carbon nanotubes/nanofibers,[55-56] to two-dimensional (2D) graphene/reduced graphene[57-59] and 3D nanocages or frameworks[60] have been added to M_2S_x electrodes to activate M_2S_x, and some of the most typical examples are shown in **Figure 6**. Similar to M–S systems, the carbon amount used in the M_2S_x electrodes is typically high, usually more than 40 wt%. Characterization of carbon content in the composite sometimes is challenging due to the unstability of M_2S_x. Out of the industrial perspective, low content of conductive carbon is required for high effective capactity of the electrode.

3.3. Adding redox mediators

On the other hand, manipulating the electrolyte is another effective approach to overcome the energy barrier of M_2S_x during the initial charging process. Redox mediators, as reversible redox couples, could oxidize the surfaces of M_2S_x particles and change their electrochemical state.[65,66] The liquid and soluble polysulfides, such as M_2S_6 and M_2S_8, are most commonly used as electrolyte additives, which not only enhance the charge transfer of solid M_2S_x, but also serve as redox mediators. Meini et al.[22] effectively reduced the Li_2S activation voltage to as low as 2.9 V by using polysulfide additives as redox mediators in the electrolyte (**Figure 7**a). Liu et al.[67] used indium triiodide (InI_3), and Yushin et al.[68] used LiI to obtain similar results by the same

principle (Figure 7b). Recently, Xiang et al.[66] used ethanol as an electrolyte additive and reduced the activation voltage to 2.85 V (Figure 7c and 7d). When decamethylferrocene, lithium iodide, and ferrocene were added as redox mediators, it is interesting that a very limited amount of Li_2S was detected after charging up to 3.6 V due to the fact that the oxidation potential of Li_2S is much lower than that of these redox mediators. Thus, the Li_2S cathodes can be fully utilized, even when charging to a low potential of 3.2 V, and high capacity retention could be obtained for long-term cycling. Manthiram and colleagues have shown that P_2S_5 can be used as an electrolyte additive in the Li_2S system, and that this removes the need for the application of a high voltage during the initial charge.[69,70] The P_2S_5 additive works by improving the electrochemical activity of Li_2S, enhancing the oxidative chemistry that creates the polysulfide charging products. Promising reversible discharge capacities of about 800 mA h g_{Li2S}^{-1} were measured and the battery retained 83% of its capacity over 80 cycles. Although these redox mediators can effectively reduce the charge overpotential, they are unstable and difficult to handle with high selectivity. Therefore, the appropriate redox mediators are not easily found for practical applications.

Many researchers also combine these strategies to realize superior battery performance. Dominko et al.[71] developed nitrogen-doped carbon-coated small Li_2S particles to lower the overpotential to 2.75 V. Wang et al.[59] synthesized a free-standing Li_2S/rGO cathode paper with embedded nanosized Li_2S particles and 0.1M Li_2S_8 was employed as additive, achieving much enhanced electrochemical performance with low overpotential for their Li_2S cathode. Apart from these, Fu et al.[72] discovered that phenyl diselenide (PDSe) could decrease the charge overpotential of Li_2S by an inductive effect. Typically, most recent research has been focused on modifying M_2S_x cathode and adding polysulfides as redox mediators in the electrolyte. To lower the

overpotential, the present results encourage further works on novel M_2S_x cathode structures and redox mediators for these systems.

4. Cathodes design

As discussed above, M_2S_x cathodes are the most important parts of M_2S_x-based M–S batteries, and researchers have put enormous effort into M_2S_x electrode design, including synthesis of M_2S_x materials and investigating the composition of M_2S_x cathodes. In this section, we will review recent designs of M_2S_x-based electrodes.

4.1. Li_2S cathodes design

Li_2S cathodes suffer from low electronic conductivity and high ionic resistivity as well as the dissolution of lithium polysulfide intermediates (Li_2S_n) into the electrolyte, resulting in fast capacity deterioration and low Coulombic efficiency. Therefore, Li_2S usually should be activated. To avoid these problems, both synthesis methods and cathodes composition optimization are influential.

4.1.1. Synthesis of the Li_2S material.

Li_2S can be directly produced by a recrystallization method through evaporating ethanol from dissolved commercial Li_2S/ethanol solution,[58,72,74] although this method is a challenging way to obtain highly uniform and controllable Li_2S particles. Ball milling is another facile strategy to prepare Li_2S, and the obtained Li_2S and its composite showed smaller particle size and higher conductivity.[20] Polysulfide dissolution, however, can be accelerated in high surface area cathodes. Yushin et al.[73] developed an *in-situ* strategy via coating polymers around freshly precipitated Li_2S nanoparticles. The uniform C–Li_2S nanocomposite particles showed excellent stability, retaining a discharge capacity of over 1200 mA h g_s^{-1} over 100 cycles at a C/5 rate. *In-situ* synthesis

is the most commonly used method to prepare Li_2S particles and to obtain composites with other materials at the same time. Other methods for *in-situ* formation of Li_2S will be discussed in detail as follows.

Compared to traditional ball milling and recrystallization methods, *in-situ* formed Li_2S has the advantages of low cost, small sizes, uniformity, and environmental friendliness. **Table 2** summarizes the electrochemical performance of Li_2S cathodes formed *via in-situ* reactions. Commonly, there are two *in-situ* ways to form Li_2S, chemical synthesis and electrochemical transformation.

4.1.1.1. Chemical synthesis: Anhydrous lithium sulfide is currently produced through endothermic carbothermal reduction reactions such as:

$$Li_2SO_{4(s)} + 2C_{(s)} \rightarrow Li_2S_{(s)} + 2CO_{2(g)} \quad (16)$$

$$Li_2CO_{3(s)} + H_2S_{(g)} \rightarrow Li_2S_{(s)} + H_2O_{(g)} + CO_{2(g)} \quad (17)$$

Carbothermic reduction of Li_2SO_4 is favourable, since it does not involve any hazardous gas (such as CS_2 or H_2S) or involve air sensitive reactants (Li_2S or Li metal).[75] Previous studies on Li_2SO_4-derived Li_2S cathodes[52] showed that the reduction temperature and carbon sources play critical roles in determining the overpotential in the first charging step, the discharge capacity, and the cycling stability of the obtained Li_2S. Different carbon sources have been used, such as polyvinyl pyrrolidone (PVP),[76,77] polyvinyl alcohol (PVA),[78] CNT,[56,79,80] sucrose,[81] chitosan,[82] and GO.[83,84] Simply mixing commercial Li_2S and CNT show negligible enhancement of electrochemical performance.[62] Therefore, the electrochemical improvement of metal sulfides/C composites via carbotherimic reduction can be attributed to the synergy between metal sulfides and carbon components. The products of metal sulfides/C composites all show improved electrochemical performance. Nonetheless, the effects of different carbon sources on the carbothermal reduction have not been clearly investigated yet.

Furthermore, even though carbothermic reduction of Li_2SO_4 can yeild Li_2S–C composites in a one-step reaction, these high-temperature processes (600−1000 °C) and problems with impurities and uniformity are matters of concern.

J. Cairns et al.[85] first reported a chemical vapour deposition (CVD) method to synthesize Li_2S spheres with size control through the reaction:

$$S + 2LiEt_3BH \rightarrow Li_2S + 2Et_3BH + H_2 \quad (18)$$

The obtained Li_2S particles with conductive carbon shell protection showed good electrochemical performance with a high first discharge capacity of 972 mA h g^{-1} Li_2S at a current rate of 0.2C. Sun et al.[86] further optimized this material by combining the Li_2S@C with single-layered graphene to form a durable protective carbon layer.

Carbon coated Li_2S can also be realized via a novel thermal reaction between gaseous carbon disulfide (CS_2) and Li metal.[87] The reaction is described by the following equation:

$$4Li(l) + CS_2(g) \rightarrow 2Li_2S(s) + C(s) \quad (19)$$

The crystalline Li_2S cores and graphene encapsulation shells have high conductivity and excellent stability. Significantly, this core-shell structure could faciliate a high mass loading of Li_2S (10 mg cm^{-2}), to show excellent electrochemical performance. Li metal is highly reactive and flammable, however, and CS_2 is highly toxic, so this reaction requires critical synthesis conditions with serious safety concerns, which is not feasible for large-scale production.

4.1.1.2. Electrochemical transformation: Recently, Zhang et al.[93] reported an electrochemical conversion process, in which Li_2S_8 catholyte could be *in-situ* converted into amorphous Li_2S. The constructed Li_2S/graphite full-cell delivered a high discharge capacity of 1006 mA h g^{-1}, indicating a high utilization of the amorphous Li_2S.

Chen et al.[94] first reported a top-down method to prepare Li_2S cathode by *in-situ* electrochemical conversion of commercial molybdenum disulfide (MoS_2) at low voltages, which worked as a high performance active material in Li-S batteries. The initial discharge process would be:

$$MoS_2 + x\ Li^+ + x\ e^- \rightarrow LixMoS_2\ (\geq 1.00V) \quad (20)$$

$$Li_xMoS_2 + (4–x)\ Li^+ + (4–x)\ e^- \rightarrow Mo + 2Li_2S\ (0.01\ V) \quad (21)$$

Followed by:

$$Li_2S \leftrightarrow S + 2Li+ + 2e^-\ (\leq 3.00\ V) \quad (22)$$

Recently, Balach et al.[92] reported a similar concept, by using hydrothermally prepared reduced graphene oxide (rGO)–covered MoS_2 particles composite as a processor. When fully lithiated and irreversible decomposed at 0.01 V, a Li_2S@rGO composite was produced *in-situ* with a high Li_2S mass loading of ~5 mg cm^{-2}.

4.1.2. Composition of Li_2S cathodes

4.1.2.1. Simple composites. Incorporate Li_2S in other materials is commonly used to solve challenges of Li_2S cathdoes for Li–S batteries.

Li_2S–C: The integration of Li_2S with carbonaceous frameworks is very common, which includes the use of carbon nanoparticles, amorphous or crystalline carbon matrices, and carbon coating. For instance Li_2S-linked multi-walled carbon nanotubes, synthesized by a facile solution-based approach, displayed better electrochemical properties than the commercial Li_2S powder.[62] Commercial bulk Li_2S particles trapped between two self-weaving carbon nanotube layers, also showed improved electronic and ionic transport and well immobilized polysulfides during cycling.[56]

Li_2S–metal: The combination of Li_2S with metal would be applicable to all solid-state Li–S batteries. In order to enhance the electrical conductivity of Li_2S cathode, attempts

such as forming Li_2S–Fe and Li_2S–Cu composites with transition metals have been explored.[95,96] Obrovac et al.[96] developed a Li_2S–Fe composite with 1:2 molar ratio by high-energy ball milling of Fe chips with Li_2S powder. The Li_2S–Fe composite was not fully activated, and thus showed unsatisfactory performance with reversible capacity of less than 292 mA h g^{-1} over three cycles at 10 mA g^{-1}. Nevertheless, the composite did show some promise for decreasing capacity fading with little overpotential. Takeuchi et al.[97] further developed a LiI-doped Li_2S–Fe composite cathode material. The dopant LiI could stabilize the composite material structure against Li insertion/extraction reactions, and suppress the side-reactions with the electrolyte simultaneously, leading to improved cycling performance.

Li_2S–other composites: Conductive carbon backbones could alleviate the problems of Li_2S to some extent. Carbon, however, being non-polar in nature, is not capable of favourable binding with highly polar Li_2S, and therefore, it is incapable of confining the intermediate Li_2S_n species during cycling. To deal with this challenge, Cui et al.[98] reported the encapsulation of Li_2S with a conducting polymer (**Figure 8**a), owing to the favorable Li–N interaction provided by the N atoms in polypyrrole (PPy) with Li_2S, the intermediate Li_2S_n species could be effectively constrained from migration by PPy with strong binding so as to cover the surface of Li_2S, while the PPy can also enhance the electronic conductivity as a conducting polymer. Therefore, the Li_2S–PPy composites showed a high capacity of 785 mA h g^{-1} over 400 cycles. Jiang et al.[99] synthesized a core-shell nano-Li_2S@Li_3PS_4 composite as a superionic conducting material (Figure 8b), Li_3PS_4 could provide protection for the Li_2S active material from the electrolyte, retard the dissolution of polysulfides, and confine the charge/discharge products of S_8 and Li_2S in a certain range. Yushin et al.[68] synthesized a novel Li_2S@$LiTiO_2$ core-shell nanocomposit (Figure 8c), according to the reaction:

$$2TiO_2 + Li_2S \rightarrow 2LiTiO_2 + S_{(g)} \quad (23)$$

The $LiTiO_2$ formed *in-situ* exhibited strong bonding to Li_2S, subsequently inducing a rapid conversion between long-chain polysulfides. The Li_2S@$LiTiO_2$ cathode offered discharge capacity of ~585 mA h g^{-1} at C/2 and a capacity retention of 92% over 200 cycles.

4.1.2.2. Composites with catalytic hosts. To date, novel polarized sulfur hosts, like metallic compounds[100,101] and metal sulfides[102,103], have been explored in Li–S batteries. Compared with non-polar carbon materials, these polarized host materials possess strong intrinsic sulfiphilic properties, which could constrain polysulfide dissolution by the strong chemical interactions between the polar host materials and the polysulfides. A similar strategy has been applied in Li_2S- based Li–S batteries.

Single atom catalysts: Single-atom catalysts (SACs) are of great interest and significance for sustainable energy applications.[104] The atomically dispersed metal catalysts not only offer maximal atomic utilization, but also provide an ideal model to help investigate the catalytic mechanism in the meantime.[105-107] Zhang and his co-workers demonstrated the compelling role of SA catalyst in boosting the electrochemical conversion process of Li_2S cathode.[108] They designed a nanostructured Li_2S cathode with uniformly distributed single iron atoms (SAFe) supported on porous nitrogen-rich carbon matrices (NC). Spectroscopic and electrochemical analysis combined with theoretical simulations (**Figure 9**a) showed that the SAFe with high catalytic activity can realize a low activation voltage of Li_2S (2.84 V) without sacrificing the current rate. A first discharge capacity of 1343 mA h g^{-1} at 0.2 C was achieved, with a capacity of 588 mA h g^{-1} even maintained at 12 C with a slight capacity fading rate of 0.06% per cycle over 1000 cycles at 5 C.

MXene: MXene, a family of 2D transition metal carbides and nitrides, has been widely used in the energy storage field.[109-111] Typically, they are synthesized by selective etching of the A element from the MAX phase by HF. The name MXene originated from its composition $M_{n+1}AX_n$; where M is a transition metal, A is an element from group IIIA or IVA, X stands for C/N, and n=1, 2, or 3.[110] Yu et al. reported that Ti_3C_2 possessed multiple functions in Li_2S cathode-based Li–S batteries.[112] As a typical MXene structure, Ti_3C_2 has a 2D layered structure similar to that of graphene. The abundant Lewis-acid Ti-sites and terminal functional groups on the surfaces of Ti_3C_2 sheets enable a Lewis acid-base interaction with polysulfides.[113,114] Through ball milling of commercial Li_2S with multi-layer (ML) Ti_3C_2, the obtained ML–Ti_3C_2/Li_2S composite cathode had an decreased activation barrier of 2.85 V, retained a discharge capacity of 450 mA h g^{-1} over 100 cycles at 0.2 C, and showed high rate capabilities of 750, 630, 540, 470 and 360 mA h g^{-1} at 0.1 C, 0.2 C, 0.5 C, 1 C, and 2 C, respectively. As illustrated in Figure 9b, the merits of the ML–Ti_3C_2 can be summarized as follows: (1) the high electronic conductivity of the 2D structures of ML–Ti_3C_2/Li_2S facilitates physical adsorption of polysulfide ions; (2) Lewis-acid Ti-sites and terminal functional groups could strongly bind with polysulfides; (3) the Ti–S bonds between Li_2S and ML–Ti_3C_2 helps to reduce the activation voltage barrier.

Metal Sulfides: Polar metal sulfides with superb polysulfide absorptivity have been employed in Li_2S cathode Li–S batteries and they have shown improved cycling stability. Manthiram et al. reported a 3D transition-metal sulfide-decorated carbon sponge (3DTSC) host with excellent eletrocatalytic and absorption activity,[115] as shown in Figure 9c, The zero-dimensional (0D) metal sulfide nanodots can maximize the aspect ratio of the active catalytic sites, thereby providing high catalytic activity and strong chemical interaction toward sulfide species. Based on these advantages, Li_2S on

the 3DTSC framework host showed a high discharge capacity of 8.44 mA h cm^{-2} at 0.1 C. Qiu et al. developed a composite consisting of ultra-small Li_2S nanocrystallites, sulfiphilic ZnS nanodots, and an N-doped porous carbon matrix (Li_2S–ZnS@NC) derived *in-situ* from Li_2SO_4 and zeolitic imidazolate framework-8 (ZIF-8),[116] as shown in Figure 9d. Benefiting from the presence of abundant ZnS catalyst, the Li_2S dissociation in Li_2S–ZnS@NC cathodes could be greatly accelerated, so that the electrode exhibited an excellent rate response to up to 8 C, a long life of 1000 cycles with scarcely any capacity decay, and a high areal capacity of 4.81 mA h cm^{-2} at a high Li_2S loading. Cui et al.[117] designed Li_2S@TiS_2 core-shell nanostructures, where the two-dimensional layered structure of TiS_2 provided effective encapsulation for Li_2S cathode to overcome the significant constraints. Manthiram and his co-workers further developed a Li_2S–TiS_2 composite cathode through a facile two-step dry-mixing and electrolyte-dispersion process.[118] The semi-metallic TiS_2 is an electrochemically active material with strong polysulfide-trapping capability that has been used in various sulfur cathode chemistries.[119,120] The Li_2S–TiS_2 composite cathode possessed close-contact and a three-phase boundary, which helped to promote the Li_2S-activation efficiency and provided fast redox-reaction kinetics. TiS_2 can also immediately adsorb any polysulfides generated from the surrounding Li_2S, compelling the Li_2S–TiS_2 cathode to maintain stable capacities at C/7 to C/3 over 500 cycles, with promising high-rate performance up to 1C.

4.2. Na_2S cathodes design

Similar to Li_2S cathodes, Na_2S cathodes also suffer from poor electronic conductivity, low ion diffusivity, and polysulfide dissolution. The design principles for Na_2S cathodes are usually borrowed from Li_2S cathodes. In 2014, Manthiram's team initiated the

research on Na_2S cathode for RT sodium–sulfur batteries.[44] As Na_2S is intrinsically inactive, they developed a cathode structure with the multi-walled carbon nanotube (MWCNT)-wrapped Na_2S particles spread onto MWCNT fabric (**Figure 10**a). The MWCNT fabric could facilitate efficient electron conduction and fast ion transport. Thus, with 1.5 M $NaClO_4$ and 0.3 M $NaNO_3$ additive solution as electrolyte, they obtained high capacity of 560 mA h g^{-1} and 380 mA h g^{-1} at C/10 and C/3 over 50 cycles, respectively. To improve the limited cycle life with a traditional porous separator in this work, they further integrated Na_2S cathode with a porous ion-selective Nafion coated porous membrane (Figure 10b).[121] Figure 10c and 10d present charge-discharge and CV profiles of a Na‖Na-Nafion/carbon nanofiber (CNF)‖Na_2S/CNF cell at 0.2 C and 0.1 mV s^{-1}. Like Li_2S, the slow initial-charge of the Na_2S/CNF cathode is supposed to be caused by the low electrical conductivity and sodium ionic diffusibility of the Na_2S material.[122] The initial charge curves exhibited a huge overpotential in both works. The Na-Nafion film could provide facile Na^+ conductive pathways to maintain the cycling stability of the cell. As Nafion membrane possesses small hydrophilic pores (< 5 nm) in a negatively charged environment, it can greatly prevent sodium polysulfide migration in the electrolyte via a “structure effect”, and an “electronic effect”. The Na_2S cathode in this work displayed capacities of ~800 mA h g^{-1}, ~ 680 mA h g^{-1}, and ~640 mA h g^{-1}, at C/10, C/5, and C/3, respectively, maintaining ~680 mA h g^{-1} over 100 cycles at C/5.

Manthiram’s works on Na_2S cathodes exhibited exciting improvements, but the rate capacity of micro-sized Na_2S still has room to improve because of its low electrochemical reactivity. Li and his co-workers developed a scalable strategy by using Na_2S-PVP methanol solution to prepare hollow Na_2S nanospheres, which were embedded in a carbon matrix. Finally, it formed an intriguing architecture, which is

similar to the morphology of frogspawn coral in Figure 10e.[123] The hollow structure of Na_2S shortens the Na^+ diffusion pathways, and its core-shell structure enhances the electron transfer from the carbon matrix. Therefore, these hollow Na_2S nanospheres showed a high initial discharge capacity of 980 mA h g^{-1}_{sulfur} at a high current densities of 1.4 A g^{-1}, retaining 600 mA h g^{-1}_{sulfur} after 100 cycles (Figure 10f).

To realize the high dispersion of Na_2S particles in the carbon matrix, Kaskel et al.[124]developed a new approach to synthesize Na_2S/C composite by carbothermal reduction of Na_2SO_4 at different temperatures:

$$Na_2SO_{4(s)} + 4C_{(s)} \rightarrow Na_2S_{(s)} + 4CO_{(g)} \qquad (24)$$

The Na_2S/C composite synthesized at 860 °C shows a stable performance with the highest discharge capacities of 740 mA h g_S^{-1} and stable CE.

4.3. K_2S_x cathodes design

Design of K_2S_x cathodes is more challenging since the variable species and unclear mechanisms. In order to investigate the mechanisms of K_2S_x cathodes, insoluble short-chain sulfides and soluble long-chain polysulfides were prepared by different methods. Wu et al.[48] synthesized two potassium sulfides, K_2S_3 and K_2S_2 via precipitation and solid-state reactions, respectively (**Figure 11**a):

$$2K + 3S \xrightarrow{20℃} K_2S_3 \qquad (25)$$

$$K_2S + K_2S_3 \xrightarrow{285℃} 2K_2S_2 \qquad (26)$$

Figure 11b and 11c show the X-ray powder diffraction (XRD) and ultraviolet-visible spectroscopy (UV-vis) spectra of as-prepared K_2S_2 and K_2S_3, respectively. To investigate the electrochemical pathways of K_2S_x ($x \leq 3$), a special cell was designed, as shown in Figure 5a. The K_2S_x was placed on the cathode side and was electrically separated from the anode (carbon paper). Impressively, the cell showed reversible

electrochemical reactions, indicating that redox active species can be formed, which is followed by dissolving and diffusing across the separator into the anode side. This indicated that K_2S_2 and K_2S_3 could be further discharged and the full theoretical capacity (1675 mA h g^{-1}) of the RT K−S batteries was achieved. Meanwhile, the further discharge of K_2S_3 is determined by the solid reaction, while the charge capacity mostly originates from the solution pathway. These unique electrochemical pathways result in the asymmetry of K–S cells. The low solubility of K_2S_3 and K_2S_2 limited the capacity of the cathode electrode, however, and in addition, the accumulation of K_2S would result in "dead polysulfide" and capacity decay.

Sun et al.[49] dissolved K and S in diethylene glycol dimethyl ether (DEGDME) with a molar ratios of 2:5 to form long-chain K_2S_x ($5 \leq x \leq 6$). The K_2S_x ($5 \leq x \leq 6$) catholyte simultaneously serve as reactive sulfur species and a K^+-conducting medium. The results showed that the solution phase polysulfide catholyte possessed better reversibility and faster reaction kinetics than the solid-phase elemental sulfur. The prepared K_2S_x battery demonstrated a high capacity of 400 mA h g^{-1} at 0.1 C with 94% capacity retention over 20 cycles and a good rate capability up to 2 C (Figure 11d).

Compare to Li_2S and Na_2S, K_2S_x deliver much lower capacity than theoretical capacity. Insoluble short-chain sulfides deliver higher capacity but sluggish reaction kinetics, while soluble long-chain polysulifdes show lower accessible capacity but higher reversibility. Based on the above results, we expect the following strategies to improve the electrochemical performance of the K_2S_x cathodes: (1) constructing a conductive framework with high surface area, preferably porous carbon, to accommodate the formation of K_2S, (2) combining solid state K_2S_x with soluble K_2S_x to get a synergistic effect.

M_2S_x cathodes, especially M_2S cathodes, suffer from low electronic conductivity and high ionic resistivity as well as the dissolution of polysulfide intermediates into the

electrolyte. The principle of M-S cathodes design is to overcome these disadvantages. M_2S_x nanometerization is the most common strategy to reduce the overpotential during the initial charging process; however, this method cannot improve their electrical conductivity and avoid polysulfide dissolution. For insoluble M_2S_x cathodes, the most promising strategy is combining nanosized M_2S_x with conductive materials, for example, CNT,[55] Graphene[57], and PPy[98]. The interaction between M_2S_x with these conductive materials will enhance their conductivity and boost electron and ionic transport; meanwhile, these composition cathodes can prevent the dissolution of polysulfides.[116] As for these soluble M_2S_x materials, such as K_2S_5 and K_2S_6, it is reckoned therefore that constructing a composite with a conductive and high surface area framework can effective inhibit their dissolution during cycling, thereby improving their electrochemical performance.[49]

In summary, the design principles for high-performance M_2S_x cathodes lie in the following aspects: (1) the dimensions of M_2S_x are expected to be uniform and nanoscaled; the synthesis processes should be low-cost and environment friendly; (2) the synthesized composites should have high electrical conductivity, ionic diffusibility, and structural stability, to enhance the electrochemical reactivity of M_2S_x, thereby improving the redox-reaction kinetics; (3) multifunctional hosts are expected to significantly activate these M_2S_x materials, which are supposed to have specific nanostructures and sulfiphilic components to constrain polysulfide dissolution.

5. Electrolytes design

Electrolytes act as the ion transport pathway between the anode and cathode. In M–S batteries, electrolytes are even more critical. A series of highly soluble metal polysulfide intermediates (M_2S_x, $4 \leq x \leq 8$) can dissolve into the electrolyte, and subsequently diffuse between the cathode and the anode, causing parasitic reactions with the metal

anode. As a consequence, the M–S battery generally demonstrates fast self- discharge, low efficiency and poor cycling stability. Moreover, the intrinsic tendency of the long-chain metal polysulfides to dissolve in organic liquid electrolytes still cannot be completely avoided at the present stage. On the other hand, a solid-state electrolyte, because of its solid interface, has better capability to avoid the dissolution and shuttling of polysulfides than a liquid electrolyte. Nevertheless, its low ionic conductivity and interfacial instability impede the wide use of solid-state electrolyte in M-S batteries.

5.1. Carbonate electrolytes

Carbonate solvents, for example ethylene carbonate (EC) and propylene carbonate (PC), usually have high ionic conductivity and electrochemical stability, as well offering favourable anode passivation. The carbonates could react, however, with reduced-solubility lithium polysulfides by nucleophilic attack during the first discharge process, which would result in the degradation of the electrolyte, loss of active material, and capacity fading.[125,126] Nevertheless, carbonate-based electrolytes have been widely used in M–S batteries, where sulfur is encapsulated or immobilized in the host materials/polymeric composites.[127-131] So far, research on M_2S_x cathode in carbonate-based electrolytes is rare. Balach et al.[91] studied the electrochemical performance of Li_2S cathode developed by a top-down approach in carbonate-based electrolyte (**Figure 12**a), by limiting the voltage window to between 0.8 and 3.0 V to avoid side-reactions. The results included a high initial capacity (975 mA h g_{Li2S}^{-1} at 0.1 C), a low degradation rate (0.18% per cycle over 200 cycles at 2 C) and notable Coulombic efficiency (~99.5%). The good performance in carbonate-based electrolyte may be attributed to the absence of the "shuttle effect" of the reduced graphene oxide-wrapped Li_2S particles. Kasel et al.[124] studied the electrochemical performance of Na_2S cathode in carbonate

electrolyte. They *in-situ* built the solid electrolyte interphase (SEI) by using a certain portion of carbonate additive, the side reaction with polysulfides and the accompanied active material loss could be efficiently suppressed. None of the K_2S_x-based S batteries used carbonate-based electrolytes. Given the decent electrochemical performance provided by the RT K–S batteries using the sulfurized PAN and the small molecular sulfur-based cathodes in carbonate electrolyte,[132] future research on K_2S_x-based S batteries can be devoted to this electrolyte system.

5.2. Ether electrolytes

Compared with the carbonate-based electrolytes, the ether-based (for example, tetraethylene glycol dimethyl ether (TEGDME) and 1, 3-dioxolane/ dimethoxymethane (DOL/DME)) electrolytes are able to enhance the redox reactions of the sulfur-based cathode, thereby providing a higher reversible capacity.[9] Because the ethers possess low viscosity and low ionic resistance, they could be integrated with alkali metal salts and then be stable against nucleophilic attack by polysulfides.[8,133] Thus, the ether-based electrolytes are widely used in most M_2S_x-based M–S batteries. For example, Manthiram et al.[41,121] and Sun et al.[49] demonstrated that Na_2S-carbon composite and K_2S_x ($5 \leq x \leq 6$) showed excellent electrochemical performance in TEGDME-based electrolyte. Li et al.[123] also indicated that Na_2S nanospheres exhibited a high capacity in diethylene glycol dimethyl ether (DEGDME) and DOL. Wu et al.[48] utilized potassium bis-(fluorosulfonyl)imide (KFSI)-DME as the electrolyte for a mechanism study of K_2S_2 and K_2S_3 to achieve a reversible anode reaction. The cells with ether electrolytes usually experience a severe shuttle effect, however, and severe self-discharging, resulting in low capacity and fast capacity decay. Therefore, massive research has been conducted to improve the performance of the liquid electrolytes in

M_2S_x-based M–S batteries. For example, Yang et al.[20] suggested that the electrochemical performance of the Li_2S cathodes could be enhanced by $LiNO_3$ and Li_2S_8 additives (Figure 12b). The improvement lies in that $LiNO_3$ is able to passivate the Li film surface, which could greatly enhancing the Coulomb efficiency. Meanwhile, the addition of polysulfides can compensate for the cathode material loss caused by side reactions on the Li film surface. Generally, Li_2S electrodes require a high voltage for activation, but ether electrolytes usually show instability above 4 V (*vs.* Li/Li^+). Therefore, Meini et al.[22] developed mediator additives to activate the Li_2S cathode, to avoid the electrolyte degradation caused by the high voltages. Recently, Xia et al.[134] reported a new strategy involving a dual-phase electrolyte to efficiently utilize Li_2S by using a ceramic lithium super-ionic conductor (LISICON) film to separate the electrolytes for the Li_2S cathode and for the anode (Figure 12c). They assumed that further charging after the formation of lithium polysulfides involved both electrochemical and chemical reactions and that the surface polysulfides (Li_2S_x, $4 \leq x \leq 8$) could be further transformed into the longer-chain polysulfides by electrochemical oxidation. Meanwhile, the solid Li_2S can also be oxidized by the longer-chain polysulfides through direct chemical reaction. Under this battery configuration, even commercially available micro-sized Li_2S could be activated and utilized with high efficiency.

5.3. Solid electrolytes (SEs)

Due to its inherent non-flammability and better electrochemical stability, a solid electrolyte (SE) would not only eliminate the problem of polysulfide dissolution, but also exhibit better safety and reliability than liquid electrolytes.[135,136] Even so, all-solid-

state batteries (ASSBs) have been plagued by the relatively low ionic conductivity of SEs and the large charge-transfer resistance between the electrodes and the SEs

5.3.1. SEs for Li_2S-based Li–S batteries

In 2008, Hayashi first reported Li_2S cathode-based all-solid-state lithium-sulfur batteries using inorganic electrolyte powders.[137] Ball-milled Li_2S–Cu composite was used as the cathode, and paired with an In anode in a Li_2S–P_2S_5 glass-ceramic electrolyte. The electrochemical performance of the In/Li_2S–P_2S_5 glass-ceramic/Li_2S–Cu full-cell was examined and showed a high first discharge capacity of about 490 mA h g^{-1}. The capacity gradually decreased during charge–discharge cycling, with a retained capacity of ~ 350 mA h g^{-1} over 20 cycles. By changing the Li_2S to Cu ratio and introducing carbon into the composite,[95] this cell could achieve superior rate capability and work at high current densities from 1280 to 12,800 μA cm^{-2} at room temperature. They further reduced the particle size of Li_2S, which is beneficial to form favourable contact among electrode components, and also improves the contact between the electrode materials and solid electrolytes.[138] The obtained In/Li_2S–P_2S_5 glass-ceramic/Li_2S full-cell exhibited a capacity of ~ 1000 mA h g^{-1} at 0.064 mA cm^{-2}, and they also tested its charge-discharge performance at a high current density of 6.4 mA cm^{-2} (3.5 C). Liang and his co-workers further designed a core-shell structure with Li_2S nanoparticles as the core and Li_3PS_4 as the shell.[139] The lithium superionic sulfide delivered an ionic conductivity of 10^{-7} S cm^{-1} at 25 °C, nearly 6 orders of magnitude higher than that of bulk Li_2S(~10^{-13} S cm^{-1}). The Li/Li_3PS_4/Li_2S@Li_3PS_3 cell showed a discharge capacity of 435 mA h g^{-1} at 1C over 30 cycles, and a reversible capacity of 720 mA h g^{-1} when further cycled at the low rate of C/10. Tatsymi et al.[140] paired Li_2S–C with a Li_3PO_4–Li_2S–SiS_2 glass electrolyte, and the In/Li_3PO_4–Li_2S–SiS_2 glass-ceramic/Li_2S–C cells showed an initial discharge capacity of 920 mA h g^{-1}, and higher

discharge capacity and Coulombic efficiency than those of the Li/Li_2S–C cells with electrolytes. In order to decrease the volume change and promote better interface contact, Wang and his co-workers reported a novel bottom-up method to synthesize a Li_2S–Li_6PS_5Cl–C nanocomposite,[141] combined with Li_6PS_5Cl (LPS) as a solid electrolyte and Li–In alloy as the anode (**Figure 13**a). The cell delivered a large reversible capacity (830 mA h g^{-1} for 60 cycles at 50 mA g^{-1}) and a high rate performance, even at a high loading (~3.6 mg cm^{-2}). Other ways can also be effective to improve the contact, including mixing Li_2S with vapour grown carbon fibre (VGCF) (Figure 13b),[142] incorporating a solvent interlayer into the electrode [143], and loading Li_2S on stainless steel mesh[144] (Figure 13c). To date, a Li_2S@C nanocomposite with Li_2S nanocrystals embedded in a carbon matrix has shown the best electrochemical performance, with a high initial charge capacity of 1209 mA h g^{-1}, a high reversible capacity of 644 mA h g^{-1} at 2 mA cm^{-2}, even after 700 cycles. Significantly, the accessible capacity is slightly higher than the theoretical value, which can be attributed to the side reaction of the sulfide solid electrolyte $Li_7P_3S_{11}$.[145]

High ionic conductivity is the main challenge for SEs.[146] Compared with sulfur compounds with ionic conductivity of ~ 10^{-6} S cm^{-1} – 10^{-4} S cm^{-1}, LISICON solid electrolyte exhibits a higher ionic conductivity of ~ 10^{-3} S cm^{-1} at room temperature, which is comparable to those of liquid electrolytes.[147] Moreover, LISICON is more stable against moisture than sulfur compounds. Kanno et al.[148] demonstrated thio-LISICON as a solid electrolyte in all solid-state Li–S batteries in 2008, and obtained high reversible capacity of 900 mA h g^{-1} at 0.013 mA cm^{-2}. It can be seen that LISICON ceramic solid electrolyte holds great promise for use in all-solid-state Li–S batteries, thus providing significant opportunities in all solid-state Li_2S-based Li–S batteries.

5.3.2 SEs for Na_2S-based RT Na–S batteries

Wang and his co-workers reported Na_3PS_4 (NPS)–Na_2S–C nanocomposite as a suitable cathode materials to address the interfacial issue for the ASSBs.[149] Mixing Na_3PS_4 with high ionic conductivity carbon could simultaneously creat a good solid electrolyte and active material (catholyte). This resulted in intrinsically superior electrode/electrolyte interfacial contact because only two phase contact would be involved for the charge transfer reaction. It was clear that nanosized Na_2S can effectively enhance the reversible capacity in contrast to microsized Na_2S (**Figure 14**a and b). In the full-cell test (Na–Sn–C composite as the anode, cubic Na_3PS_4 as the solid electrolyte, and Na_3PS_4–Na_2S–C nanocomposite as the cathode), it exhibited a high first discharge capacity of 869.2 mA h g^{-1} at 50 mA g^{-1} between 0.5–3.0 V at 60 °C (Figure 14c). This result is a significant step toward high-performance ASSBs for practical applications. Nevertheless, it is worth noting that the above Na_3PS_4 SEs were fabricated by a cold-pressing process, which left high residual stress. In addition, the large volume changes of S/Na_2S during cycling would induce additional stress, which further seriously weakened the lower-contact interfaces among the active materials, the solid electrolyte, and the electron conductive agent. To reduce the interface resistance and remove the residual stress in Na_2S cathodes, they further developed Na_2S–Na_3PS_4–CMK-3 nanocomposite by using a melt-casting method followed by an annealing-precipitation method.[54] This casting-annealing process guaranteed close interfacial contact between the Na_3PS_4 solid electrolyte and the CMK-3 mesoporous carbon, which, in turn, served as a favourable matrix with mixed high ionic/electronic conductivity. On the other hand, the Na_2S active species *in-situ* grown from the solid electrolyte guaranteed interfacial contact among these three subcomponents without residual stress, which greatly reduced the interfacial resistance and improved its cycling performance. Na_3PS_4 was formed by the reaction in Eq. 27:

$$3Na_2S + P_2S_5 \rightarrow 2Na_3PS_4 \quad (27)$$

The Na_2S–Na_3PS_4–C composite cathode paired with Na-Sn alloy anode and $0.75Na_2S{\cdot}0.25P_2S_5$ glass ceramic (Na_3PS_4) as the solid electrolyte achieved a discharge capacity of > 800 mA h g^{-1} in the initial cycle (Figure 14d) and high reversible capacity of > 650 mA h g^{-1} at 50 mA g^{-1} over 50 cycles at 60 °C (Figure 14e and 14f).

The development of ASSBs suitable for RT Na–S batteries is still stagnant due to the limited effectiveness and applications of these techniques. A leap forward in progress on ASSBs must be accompanied by a revolution in electrode/electrolyte interface technology or battery design, to solve the interfacial problem and simplify the preparation process for the cathode, resulting in better performance, easier preparation, and lower cost.

To date, there is no research reported with solid electrolytes for RT K–S batteries. However, we could get enlightened from researches on solid electrolytes for RT M–S batteries. Unlike the large number of Li^+ and Na^+ conductive compounds used for SE, including both oxides and sulfides, the number of K^+ conductive compounds for inorganic SE is scanty. Developing K^+ compounds with high ionic conductivity, such as potassium thiophosphate superionic conductors, will provide new research opportunities for future K–S batteries.

Table 3 summarized the advantages and drawbacks for different types of electrolytes used in M_2S_x-based M–S battery systems. Carbonate and ether electrolytes have the advantages of high ionic conductivity and interfacial stability, which tend to achieve high electrochemical performance in terms of reversible capacity, rate capability, and cycling lifespan. In contrast, solid state electrolytes possess high electrochemical and thermal stability but inferior ionic conductivity. Even though the battery performance with solid

state electrolytes is unsatisfactory, the restriction of polysulfides dissolution and nonflammability make them attractive for M_2S_x-based M–S battery systems.

6. Anodes

Most of the research related to M–S batteries based on alkali-metal sulfide cathodes is also based on alkali metal/metal alloy anode, which we usually call a "half-cell" configuration. In the pursuit of high safety, much attention has been paid to replacing alkali metals with active metal-free anode materials that can react with M ions, such as C, Si, P, and Sn based materials.

6.1. Alkali Metals

With their ultra-high capacity, alkali metals are typically employed as the standard anodes to investigate the fundamental electrochemical performance of the as-prepared alkali-metal sulfide composite cathode materials. Nevertheless, metallic alkali metals suffer from inferior stripping/plating performance, and there are serious safety concerns due to their high reactivity and flammable properties.[13] This issue is made even worse in the M–S battery system due to the so called "shuttle effect", in which the dissolved high-order polysulfides would react with metal ions at the surfaces of metal anodes. The Na_2S_x and K_2S_x systems in particular encounter much bigger challenges, because of the stronger metallic activity and the use of carbonate electrolytes without proper additives. Some researches tried to impregnate alkali-metal in carbon host to minimise the safety concern. The potassium impregnated-HC|K_2S_x ($5 \leq x \leq 6$) catholyte|3D-FCN full cell exhibited excellent reversibility and delivered a high initial discharge capacity of 235 mA h g−1 at 0.1 C (1C = 558 mA g^{-1}).[49]

6.2. Carbonaceous anodes

Carbon-based materials, because of their low cost, stability, and good intercalation and de-intercalation reversibility, have been recognized as excellent anode materials for M-ion batteries.[150] It is well-known that graphite is an excellent negative electrode materials in LIBs. The reaction mechanism between lithium and graphite, following an intercalation/de-intercalation process, has been extensively studied by various analytical techniques.[151] Zhang et al.[93] designed an amorphous Li_2S cathode formed *in-situ* to pair with a graphite anode. The full-cell delivered a high initial discharge capacity of 1006 mA h g^{-1} at 0.2C and a long cycle life over 500 cycles, indicating high utilization of the amorphous Li_2S as cathode (**Figure 15**a). Similarly, Yushin et al.[68] paired a Li_2S@$LiTiO_2$ cathode with a graphite anode and realized a capacity of 1325 mA h g^{-1}, 1242 mA h g^{-1}, 1089 mA h g^{-1}, and 975 mA h g^{-1} at C/20, C/10, C/5, and C/2, respectively, demonstrating a very promising rate performance and small voltage hysteresis.

6.3. Alloying/de-alloying materials

Alloy-type anode materials such as Si, Ge and Sn have been extensively studied both in M-ion and in M_2S_x-based M–S batteries due to their high capacity. Si, because of its high specific capacity and low discharge potential, has been recognised as a promising candidate to replace graphite.[152] More importantly, its abundance and environmental benignity make Si one of the most attractive anode materials. For example, Cui et al.[153] reported pairing Li_2S cathode with Si anode. The Li_2S/Si battery had a theoretical specific energy of 1550 W h kg^{-1}, which is four times higher than those of the $LiCoO_2$/graphite or $LiFePO_4$/graphite systems (Figure 15b). Xie et al.[88] further prepared a Li_2S@C composite cathode to couple with prelithiated Si anode. The Li_2S@C/Si battery demonstrated an initial specific energy of 630 W h kg^{-1} at 1/8 C with respect to active materials only. Another commonly studied alloy-type anode is tin, as Sn

possesses a high theoretical capacity, both by weight and by volume.[154,155] The Li_2S/Sn battery hold a theoretical specific energy of around 900 W h kg^{-1}. In order to show its safety advantage, Li et al.[123] paired a hollow nano-Na_2S composite cathode with a Sn@C composite anode, as displayed in Figure 15c, which shows the galvanostatic charge-discharge curves of the Sn@C/hollow nano-Na_2S full-cell, delivering a first discharge capacity of 550 mA h g_S^{-1} with a capacity retention of 80% over 50 cycles.

6.4 Other anodes

The Fe_3O_4//Li_2S full-cell may deliver a theoretical specific energy of around 670 W h kg^{-1}, which is 2–3 times higher than that of the best intercalation compound cathodes based LIBs. [77] Qiu et al. further studied Li_2S@CNF paper paired with prelithiated Fe_3O_4 anode. [77] The Li_2S@CNF||Fe_3O_4 full-cell delivered a high first discharge capacity of 576 mA h g^{-1}, with a specific energy of 403 W h kg^{-1}, which was capable of lighting a light-emitting diode (LED) array panel (Figure 15d). Manthiram et al.[158] developed a novel "anode-host-free" full-cell configuration formed by a Li_2S cathode and bare copper foil on the anode side (Figure 15e). The Li || Li_2S half-cell and the Cu || Li_2S full-cell showed discharge capacities of 1001 and 919 mA h g_S^{-1}at C/10, respectively. The lithium-limited nature of this configuration makes it an ideal template for achieving a fundamental understanding of the dynamics of lithium degradation and SEI formation in Li–S batteries.

Table 4 summarizes and lists the published works on alkali-metal sulfide full-cell systems. In contrast to the M_2S_x/M half-cells, the M_2S_x-based full-cells tend to show much more serious capacity decay. This could be caused by the following factors: (1) Limited supply of M ions. This can be intensified by irreversible loss due to side reactions. In half-cells, abundant M ions could be replenished by the alkali-metal

counter electrode. (2) Voltage control of full-cells. The M_2S_x cathodes or anodes may be overcharged/deep-discharged, which is pernicious to the cycling performance. (3) Volume changes in metal-free anodes. Besides the theoretical capacity and redox potential, minimal volume change also needs to be taken into account in seeking for feasible anode materials. In order to realize M_2S_x-based M–S battery systems with high specific energy density and high safety, researches on high-performance anodes are also of great significance. Ideally, the anodes are supposed to possess high theoretical capacity, proper voltage window, and stable cycling performance. Meanwhile, practically achievable full-cell configurations are required.

7. Summary and perspectives

In summary, recent progress and key issues in current alkali-metal sulfide cathode based M–S batteries have been systematically reviewed. Alkali-metal sulfide cathodes are currently limited by the high potential barrier caused by their low electrical and ionic conductivity, as well as polysulfide dissolution and the associated self-discharge and shuttle effects. In order to overcome such challenges, different activation methods, including reducing the size of the M_2S_x particles, adding conductive carbon to the electrode, and adding redox mediators to the electrolytes, have been summarized. In addition, the M_2S_x electrode design, including the synthesis of M_2S_x and the components of M_2S_x electrode, have been discussed. Electrolyte modifications, including the use of salt additives (lithium nitrate, lithium iodide, alkali-metal polysulfides, phosphorus pentasulfide, etc.), dual-phase electrolytes, and all-solid-state electrolytes, have successfully reduced the dissolution and shuttling of polysulfides, and led to very promising cycling performance. Research effort on all-solid-state electrolytes have

shown the great promise of alkali-metal sulfide cathodes for use in all-solid-state M–S batteries.

Despite the recent progress on M_2S_x-based M–S batteries, this research direction is still encountering many challenges and opportunities in terms of cathode design, electrolyte optimization, anode selection/matching, full-cell integration, and solid-electrolyte interface regulation. Specifically, future research efforts could be productively spent as follows.

(1) Future research on the Li_2S cathode should focus on the facile and scalable synthesis of Li_2S and optimization of the Li_2S electrode composition and structure. Accordingly, more effectively catalytic hosts could be explored.

(2) Graphite and silicon are the most commonly used non-metal anode materials for Li_2S-based full-cells. The specific capacity of a Li_2S full-cell usually decays faster than the specific capacity of a Li_2S/Li half-cell. Future research should devote more effort to cell configuration and voltage regulation.

(3) In contrast to the research on Li_2S, studies on Na_2S_x and K_2S_x cathodes are still in their very early stages. By borrowing the experience in Li_2S cathode, more and more fundamental research are expected. Great efforts should be made to catch up with the pace of Li_2S-based Li–S batteries in the near future. On the other hand, the anode selection varies in different systems. Promising anodes can be P and Sn for Na_2S-based Na–S batteries, while hard carbon is very attractive for K_2S_x-based K–S batteries.

(4) To date, most of the research on M_2S_x cathodes has involved ether-based electrolytes. Research on other electrolytes, especially carbonate-based electrolytes and gel-solid electrolytes, should be considered. Moreover, new electrolyte additives that are low-cost and highly stable should be developed.

(5) Due to the dissolution of various polysulfide intermediates, the M–S battery system is very complex with unclear conversion processes. Advanced characteristic techniques, including in-situ X-ray diffraction, X-ray adsorption spectroscopy, Raman spectroscopy, and UV-vis spectroscopy, are required to reveal Na-/K-storage mechanisms, leading to an in-depth understanding of the electrode/electrolyte interface.

Acknowledgements

This research was supported by the Australian Research Council (ARC) (DE170100928), the Commonwealth of Australia through the Automotive Australia 2020 Cooperative Research Centre (Auto CRC), and an Australian Renewable Energy Agency (ARENA) Project (G00849). The authors also thank Dr. Tania Silver for her critical reading of the manuscript.

Conflict of Interest

The authors declare no conflict of interest.

References

[1] N. Yabuuchi, K. Kubota, M. Dahbi, S. Komaba, *Chem. Rev.* **2014**, *114*, 11636.

[2] L. G. Lu, X. B. Han, J. Q. Li, J. F. Hua, M. G. Ouyang, *J. Power Sources* **2013**, *226*, 272.

[3] P. G. Bruce, S. A. Freunberger, L. J. Hardwick, J. M. Tarascon, *Nat. Mater.* **2011**, *11*, 19.

[4] Q. Pang, X. Liang, C. Y. Kwok, L. F. Nazar, *Nat. Energy* **2016**, *1*, 16132.

[5] G. Wang, X. Shen, J. Yao, J. Park, *Carbon* **2009**, *47*, 2049.

[6] M. Wild, L. O'Neill, T. Zhang, R. Purkayastha, G. Minton, M. Marinescu, G. J. Offer, *Energy Environ. Sci.* **2015**, *8*, 3477.

[7] H. Li, *Joule* **2019**, *3*, 911.

[8] S. S. Zhang, *J. Power Sources* **2013**, *231*, 153.

[9] A. Manthiram, Y. Fu, S. H. Chung, C. Zu, Y. S. Su, *Chem. Rev.* **2014**, *114*, 11751.

[10] R. P. Fang, S. Y. Zhao, Z. H. Sun, D. W. Wang, H. M. Cheng, F. Li, *Adv. Mater.* **2017**, *29*, 1606823.

[11] Q. Zhao, Y. Hu, K. Zhang, J. Chen, *Inorg. Chem.* **2014**, *53*, 9000.

[12] F. Cheng, J. Chen, *Chem. Soc. Rev.* **2012**, *41*, 2172.

[13] X. B. Cheng, R. Zhang, C. Z. Zhao, Q. Zhang, *Chem. Rev.* **2017**, *117*, 10403.

[14] Q. Zhang, F. Li, J.-Q. Huang, H. Li, *Adv. Funct. Mater.* **2018**, *28*, 1804589.

[15] B. W. Zhang, Y. D. Liu, Y. X. Wang, L. Zhang, M. Z. Chen, W. H. Lai, S. L. Chou, H. K. Liu, S. X. Dou, *ACS Appl. Mater. Interfaces* **2017**, *9*, 24446.

[16] X. Hong, J. Mei, L. Wen, Y. Tong, A. J. Vasileff, L. Wang, J. Liang, Z. Sun, S. X. Dou, *Adv. Mater.* **2019**, *31*, 1802822.

[17] H. Jha, I. Buchberger, X. Cui, S. Meini, H. A. Gasteiger, *J. Electrochem. Soc.* **2015**, *162*, A1829.

[18] S. C. Wu, G. M. Zhou, E. Y. Mao, Y. M. Sun, B. F. Liu, L. Wang, J. Y. Wang, F. F. Shi, Y. Cui, *Nano Res.* **2020**, *1*, 6.

[19] L. T. Zhou, W. K. Zhang, Y. F. Wang, S. Liang, Y. P. Gan, H. Huang, J. Zhang, Y. Xia, C. Liang, *J. Chem.* **2020**, *2020*, 6904517.

[20] Y. Yang, G. Zheng, S. Misra, J. Nelson, M. F. Toney, Y. Cui, *J. Am. Chem. Soc.* **2012**, *134*, 15387.

[21] F. Wu, J. T. Lee, F. Fan, N. Nitta, H. Kim, T. Zhu, G. Yushin, *Adv. Mater.* **2015**, *27*, 5579.

[22] S. Meini, R. Elazari, A. Rosenman, A. Garsuch, D. Aurbach, *J. Phys. Chem. Lett.* **2014**, *5*, 915.

[23] Y. Z. Fu, C. X. Zu, A. Manthiram, *JACS*, **2013**, *135*, 18044.

[24] M. J. Klein, A. Dolocan, C. X. Zu, A. Manthiram, *Adv. Energy Mater.* **2017**, *20*, 1701122.

[25] F. X. Wu, J. T. Lee, E. B. Zhao, B. Zhang, G. Yushin, *ACS Nano* **2016**, *10*, 1333.

[26] Y. Fu, Y.-S. Su, A. Manthiram, *Adv. Energy Mater.* **2014**, *4*, 1300655.

[27] H. J. Peng, J. Q. Huang, X. Y. Liu, X. B. Cheng, W. T. Xu, C. Z. Zhao, F. Wei, Q. Zhang, *J. Am. Chem. Soc.* **2017**, *139*, 8458.

[28] C. Shen, P. Andrei, J. P. Zheng, *ACS Appl. Energy Mater.***2019**, *2*, 3860.

[29] G. M. Zhou, E. Paek, G. S. Hwang, A. Manthiram, *Adv. Energy Mater.* **2016**, *6*, 1501355.

[30] Y. M. Sun, H. W. Lee, Z. W. Seh, G. Y. Zheng, J. Sun, Y. B. Li, Y. Cui, *Adv. Energy Mater.* **2016**, *6*, 1600154.

[31] G. Zhou, J. Sun, Y. Jin, W. Chen, C. Zu, R. Zhang, Y. Qiu, J. Zhao, D. Zhuo, Y. Liu, X. Tao, W. Liu, K. Yan, H. R. Lee, Y. Cui, *Adv. Mater.* **2017**, 1603366.

[32] Z. J. Li, Y. C. Zhou, Y. Wang, Y. C. Lu, *Adv. Energy Mater.* **2019**, *9*, 1802207.

[33] J. C. Jiang, Q. N. Fan, S. L. Chou, Z. P. Guo, K. Konstantinov, H. K. Liu, J. Z. Wang, *Small* **2019**, 1903934.

[34] A. K. Haghi, D. Balkose, S. Thomas, in *Applied Physical Chemistry with Multidisciplinary*, Apple Academic Press, New York, America, 2018, ch. 6.

[35] K. T. Schutt, H. E. Sauceda, P. J. Kindermans, A. Tkatchenko, K. R. Muller, *J. Chem. Phys.* **2018**, *148*, 241722.

[36] J. Sanster, A. D. Pelton, *J. Phase Equilib.* **1997**, *18*, 89.

[37] E. Rosen, R. Tegman, *Acta Chem. Scand.* **1971**, *25*, 3329.

[38] G. J. Janz, J. W. Coutts, J. R. Downey, E. Roduner, *Inorg. Chem.* **1976**, *15*, 1755.

[39] Z. Li, J. Zhang, X. W. Lou, *Angew Chem. Int. Ed.* **2015**, *54*, 12886.

[40] Y. W. Wu, T. Momma, H. Nara, T. Hang, M. Li, T. Osaka, *J. Electrochem. Soc.* **2020**, *167*, 020531.

[41] M. Li, Z. Chen, T. Wu, J. Lu, *Adv. Mater.* **2018**, *30*, 1801190.

[42] S. Q. Li, D. Leng, W. Y. Li, L. Qie, Z. H. Dong, Z. Q. Cheng, Z. Y. Fan, *Energy Storage Mater.* **2020**, *27*, 279.

[43] J. Y. Koh, M.-S. Park, E. H. Kim, B. O. Jeong, S. Kim, K. J. Kim, J. G. Kim, Y. J. Kim, Y. J. Jung, *J. Electrochem. Soc.* **2014**, *161*, A2133.

[44] X. Yu, A. Manthiram, *Chem. –Eur. J.* **2015**, *21*, 4233.

[45] L. Medenbach, P. Adelhelm, *Top. Curr. Chem.* **2017**, *375*, 81

[46] J. Ding, H. Zhang, W. J. Fan, C. Zhong, W. B. Hu, D. Mitlin, *Adv. Mater.* **2020**, *1*, 1908007.

[47] Y. Liu, W. Wang, J. Wang, Y. Zhang, Y. Zhu, Y. Chen, L. Fu, Y. Wu, *Chem. Commun.* **2018**, *54*, 2288.

[48] S. Gu, N. Xiao, F. Wu, Y. Bai, C. Wu, Y. Wu, *ACS Energy Lett.* **2018**, *3*, 2858.

[49] J.-Y. Hwang, H. M. Kim, C. S. Yoon, Y.-K. Sun, *ACS Energy Lett.* **2018**, *3*, 540.

[50] L. Chen, Y. Liu, M. Ashuri, C. Liu, L. L. Shaw, *J. Mater. Chem. A* **2014**, *2*, 18026.

[51] K. Cai, M. K. Song, E. J. Cairns, Y. Zhang, *Nano Lett.* **2012**, *12*, 6474.

[52] J. Liu, H. Nara, T. Yokoshima, T. Momma, T. Osaka, *Electrochim. Acta* **2015**, *183*, 70.

[53] Y. Z. Zhao, Y. G. Yang, C. A. Wolden, *ACS Appl. Energy Mater.* **2019**, *2*, 2246.

[54] X. Fan, J. Yue, F. Han, J. Chen, T. Deng, X. Zhou, S. Hou, C. Wang, *ACS Nano* **2018**, *12*, 3360.

[55] F. Li, C. Wu, J. C. Jiang, H. K. Liu, J. Z. Wang, *J. Alloys Compd.* **2020**, *828*, 154264.

[56] M. Wu, Y. Cui, Y. Fu, *ACS Appl. Mater. Interfaces* **2015**, *7*, 21479.

[57] K. Han, J. M. Shen, C. M. Hayner, H. Q. Ye, M. C. Kung, H. H. Kung, *J. Power Sources* **2014**, *251*, 331.

[58] J. He, Y. Chen, W. Lv, K. Wen, P. Li, F. Qi, Z. Wang, W. Zhang, Y. Li, W. Qin, W. He, *J. Power Sources* **2016**, *327*, 474.

[59] C. Wang, X. Wang, Y. Yang, A. Kushima, J. Chen, Y. Huang, J. Li, *Nano Lett.* **2015**, *15*, 1796.

[60] F. Ye, Y. Hou, M. Liu, W. Li, X. Yang, Y. Qiu, L. Zhou, H. Li, Y. Xu, Y. Zhang, *Nanoscale* **2015**, *7*, 9472.

[61] F. Wu, J. T. Lee, A. Magasinski, H. Kim, G. Yushin, *Part. Part. Syst. Char.* **2014**, *31*, 639.

[62] F. Wu, A. Magasinski, G. Yushin, *J. Mater. Chem. A* **2014**, *2*, 6064.

[63] Y. Kim, H. Han, Y. Noh, J. Bae, M. H. Ham, W. B. Kim, *ChemSusChem* **2019**, *12*, 824.

[64] L. Suo, Y. Zhu, F. Han, T. Gao, C. Luo, X. Fan, Y.-S. Hu, C. Wang, *Nano Energy* **2015**, *13*, 467.

[65] X. Liang, C. Hart, Q. Pang, A. Garsuch, T. Weiss, L. F. Nazar, *Nat. Commun.* **2015**, *6*, 5682.

[66] X. Liang, J. Yun, K. Xu, P. Shi, Y. Sun, C. Chen, H. Xiang, *Chem. Commun.* **2019**, *55*, 11088.

[67] M. Liu, Y. X. Ren, H. R. Jiang, C. Luo, F. Y. Kang, T. S. Zhao, *Nano Energy* **2017**, *40*, 240.

[68] F. Wu, T. P. Pollard, E. Zhao, Y. Xiao, M. Olguin, O. Borodin, G. Yushin, *Energy Environ. Sci.* **2018**, *11*, 807.

[69] G. Armstrong, *Nat. Chem.* **2015**, *7*,8.

[70] C. Zu, M. Klein, A. Manthiram, *J. Phys. Chem. Lett.* **2014**, *5*, 3986.

[71] A. Vizintin, L. Chabanne, E. Tchernychova, I. Arčon, L. Stievano, G. Aquilanti, M. Antonietti, T.-P. Fellinger, R. Dominko, *J. Power Sources* **2017**, *344*, 208.

[72] Q. Fan, B. Li, Y. Si, Y. Fu, *Chem. Commun.* **2019**, *55*, 7655.

[73] F. Wu, H. Kim, A. Magasinski, J. T. Lee, H.-T. Lin, G. Yushin, *Adv. Energy Mater.* **2014**, *4*, 1400196.

[74] J. He, Y. Chen, W. Lv, K. Wen, C. Xu, W. Zhang, Y. Li, W. Qin, W. He, *ACS Nano* **2016**, *10*, 10981.

[75] J. Shi, J. Zhang, Y. Zhao, Z. Yan, N. Hart, J. Guo, *Front. Energy Res.* **2019**, *7*, 53.

[76] J. Zhang, Y. Shi, Y. Ding, L. Peng, W. Zhang, G. Yu, *Adv. Energy Mater.* **2017**, *7*, 1602876.

[77] M. Yu, Z. Wang, Y. Wang, Y. Dong, J. Qiu, *Adv. Energy Mater.* **2017**, *7*, 1700018.

[78] F. Ye, H. Noh, J. Lee, H. Lee, H.-T. Kim, *J. Mater. Chem. A* **2018**, *6*, 6617.

[79] Y. Peng, Y. Zhang, Z. Wen, Y. Wang, Z. Chen, B.-J. Hwang, J. Zhao, *Chem. Eng. J.* **2018**, *346*, 57.

[80] S. Zhang, M. Liu, F. Ma, F. Ye, H. Li, X. Zhang, Y. Hou, Y. Qiu, W. Li, J. Wang, J. Wang, Y. Zhang, *J. Mater. Chem. A* **2015**, *3*, 18913.

[81] D. H. Wang, X. H. Xia, D. Xie, X. Q. Niu, X. Ge, C. D. Gu, X. L. Wang, J. P. Tu, *J. Power Sources* **2015**, *299*, 293.

[82] D. H. Wang, D. Xie, T. Yang, Y. Zhong, X. L. Wang, X. H. Xia, C. D. Gu, J. P. Tu, *J. Power Sources* **2016**, *331*, 475.

[83] Y. Chen, S. Lu, J. Zhou, W. Qin, X. Wu, *Adv. Funct. Mater.* **2017**, *27*, 1700987.

[84] Y. Chen, S. Lu, J. Zhou, X. Wu, W. Qin, O. Ogoke, G. Wu, *J. Mater. Chem. A* **2017**, *5*, 102.

[85] C. Nan, Z. Lin, H. Liao, M. K. Song, Y. Li, E. J. Cairns, *J. Am. Chem. Soc.* **2014**, *136*, 4659.

[86] D. Sun, Y. Hwa, Y. Shen, Y. Huang, E. J. Cairns, *Nano Energy* **2016**, *26*, 524.

[87] G. Tan, R. Xu, Z. Xing, Y. Yuan, J. Lu, J. Wen, C. Liu, L. Ma, C. Zhan, Q. Liu, T. Wu, Z. Jian, R. Shahbazian-Yassar, Y. Ren, D. J. Miller, L. A. Curtiss, X. Ji, K. Amine, *Nat. Energy* **2017**, *2*, 17090.

[88] X. Chen, L. Peng, L. Yuan, R. Zeng, J. Xiang, W. Chen, K. Yuan, J. Chen, Y. Huang, J. Xie, *J. Energy Chem.* **2019**, *37*, 111.

[89] Y. Qiu, G. Rong, J. Yang, G. Li, S. Ma, X. Wang, Z. Pan, Y. Hou, M. Liu, F. Ye, W. Li, Z. W. Seh, X. Tao, H. Yao, N. Liu, R. Zhang, G. Zhou, J. Wang, S. Fan, Y. Cui, Y. Zhang, *Adv. Energy Mater.* **2015**, *5*, 1501369.

[90] K. Zhang, L. Wang, Z. Hu, F. Cheng, J. Chen, *Sci. Rep.* **2014**, *4*, 6467.

[91] H. Yan, H. Wang, D. Wang, X. Li, Z. Gong, Y. Yang, *Nano Lett.* **2019**, *19*, 3280.

[92] M. Zensich, T. Jaumann, G. M. Morales, L. Giebeler, C. A. Barbero, J. Balach, *Electrochim. Acta* **2019**, *296*, 243.

[93] F. Ye, M. Liu, X. Yan, J. Li, Z. Pan, H. Li, Y. Zhang, *Small* **2018**, *14*, 1703871.

[94] X. Fang, X. Guo, Y. Mao, C. Hua, L. Shen, Y. Hu, Z. Wang, F. Wu, L. Chen, *Chem. Asian J.* **2012**, *7*, 1013.

[95] A. Hayashi, R. Ohtsubo, M. Tatsumisago, *Solid State Ion.* **2008**, *179*, 1702.

[96] M. N. Obrovac, J. R. Dahn, *Electrochem. Solid-State Lett.* **2002**, *5*, A70.

[97] T. Takeuchi, H. Kageyama, K. Nakanishi, H. Kiuchi, M. Katayama, Y. Inada, T. Ohta, T. Fukunaga, H. Sakaebe, H. Kobayashi, E. Matsubara, *J. Electrochem. Soc.* **2018**, *166*, A5231.

[98] Z. W. Seh, H. Wang, P.-C. Hsu, Q. Zhang, W. Li, G. Zheng, H. Yao, Y. Cui, *Energy Environ. Sci.* **2014**, *7*, 672.

[99] Z. Jiao, L. Chen, J. Si, C. Xu, Y. Jiang, Y. Zhu, Y. Yang, B. Zhao, *J. Power Sources* **2017**, *353*, 167.

[100] J. Zhou, X. Liu, L. Zhu, J. Zhou, Y. Guan, L. Chen, S. Niu, J. Cai, D. Sun, Y. Zhu, J. Du, G. Wang, Y. Qian, *Joule* **2018**, *2*, 2681.

[101] Y.-J. Li, J.-M. Fan, M.-S. Zheng, Q.-F. Dong, *Energy Environ. Sci.* **2016**, *9*, 1998.

[102] S. Luo, C. Zheng, W. Sun, Y. Wang, J. Ke, Q. Guo, S. Liu, X. Hong, Y. Li, W. Xie, *Electrochim. Acta* **2018**, *289*, 94.

[103] M. Wang, L. Fan, X. Wu, Y. Qiu, B. Guan, Y. Wang, N. Zhang, K. Sun, *J. Mater. Chem. A* **2019**, *7*, 15302.

[104] B. W. Zhang, T. Sheng, Y. D. Liu, Y. X. Wang, L. Zhang, W. H. Lai, L. Wang, J. Yang, Q. F. Gu, S. L. Chou, H. K. Liu, S. X. Dou, *Nat. Commun.* **2018**, *9*, 4082.

[105] B. W. Zhang, Y. X. Wang, S. L. Chou, H. K. Liu, S. X. Dou, *Small Methods* **2019**, *3*, 1800497.

[106] S. L. Chou, Y. Wu, Q. Zhang, Y. M. Kang, *Small Methods* **2019**, *3*, 1900523.

[107] B.-W. Zhang, T. Sheng, Y.-X. Wang, S. Chou, K. Davey, S.-X. Dou, S.-Z. Qiao, *Angew. Chem. Int. Ed.* **2019**, *131*, 1498.

[108] J. Wang, L. Jia, J. Zhong, Q. Xiao, C. Wang, K. Zang, H. Liu, H. Zheng, J. Luo, J. Yang, H. Fan, W. Duan, Y. Wu, H. Lin, Y. Zhang, *Energy Storage Mater.* **2018**, *8*, 246.

[109] X. Tang, X. Guo, W. Wu, G. Wang, *Adv. Energy Mater.* **2018**, *8*, 1801897.

[110] M. Naguib, V. N. Mochalin, M. W. Barsoum, Y. Gogotsi, *Adv. Mater.* **2014**, *26*, 992.

[111] O. Mashtalir, M. Naguib, V. N. Mochalin, Y. Dall'Agnese, M. Heon, M. W. Barsoum, Y. Gogotsi, *Nat. Commun.* **2013**, *4*, 1716.

[112] X. Liang, J. Yun, K. Xu, H. Xiang, Y. Wang, Y. Sun, Y. Yu, *J. Energy Chem.* **2019**, *39*, 176.

[113] W. Bao, D. Su, W. Zhang, X. Guo, G. Wang, *Adv. Funct. Mater.* **2016**, *26*, 8746.

[114] X. Liang, A. Garsuch, L. F. Nazar, *Angew. Chem. Int. Ed.* **2015**, *54*, 3907.

[115] J. He, Y. Chen, A. Manthiram, *Adv. Energy Mater.* **2019**, *9*, 1900584.

[116] M. Yu, S. Zhou, Z. Wang, W. Pei, X. Liu, C. Liu, C. Yan, X. Meng, S. Wang, J. Zhao, J. Qiu, *Adv. Funct. Mater.* **2019**, 1905986.

[117] Z. W. Seh, J. H. Yu, W. Li, P. C. Hsu, H. Wang, Y. Sun, H. Yao, Q. Zhang, Y. Cui, *Nat. Commun.* **2014**, *5*, 5017.

[118] S.-H. Chung, A. Manthiram, *Adv. Energy Mater.* **2019**, 1901397.

[119] M. S. Whittingham, *Science* **1976**, *192*, 1126.

[120] A. Berger, A. T. S. Freiberg, A. Siebel, R. Thomas, M. U. M. Patel, M. Tromp, H. A. Gasteiger, Y. Gorlin, *J. Electrochem. Soc.* **2018**, *165*, A1288.

[121] X. Yu, A. Manthiram, *Chem. Mater.* **2016**, *28*, 896.

[122] X. Yu, A. Manthiram, *Adv. Energy Mater.* **2015**, *5*, 1500350.

[123] C. Wang, H. Wang, X. Hu, E. Matios, J. Luo, Y. Zhang, X. Lu, W. Li, *Adv. Energy Mater.* **2018**, *9*, 1803251.

[124] L. M. Bloi, J. Pampel, S. Dörfler, H. Althues, S. Kaskel, *Adv. Energy Mater.* **2020**, *10*, 1903245.

[125] Z. Li, L. Yuan, Z. Yi, Y. Sun, Y. Liu, Y. Jiang, Y. Shen, Y. Xin, Z. Zhang, Y. Huang, *Adv. Energy Mater.* **2014**, *4*, 1301473.

[126] M. R. Kaiser, S. Chou, H. K. Liu, S. X. Dou, C. Wang, J. Wang, *Adv. Mater.* **2017**, *29*, 1700449.

[127] X. Li, M. Banis, A. Lushington, X. Yang, Q. Sun, Y. Zhao, C. Liu, Q. Li, B. Wang, W. Xiao, C. Wang, M. Li, J. Liang, R. Li, Y. Hu, L. Goncharova, H. Zhang, T. K. Sham, X. Sun, *Nat. Commun.* **2018**, **9**, 4509.

[128] Q. Zhu, Q. Zhao, Y. An, B. Anasori, H. Wang, B. Xu, *Nano Energy* **2017**, *33*, 402.

[129] R. Carter, L. Oakes, A. Douglas, N. Muralidharan, A. P. Cohn, C. L. Pint, *Nano Lett.* **2017**, *17*, 1863.

[130] Y. X. Wang, W. H. Lai, S. L. Chou, H. K. Liu, S. X. Dou, *Adv. Mater.* **2019**, 1903952.

[131] Y. X. Wang, W. H. Lai, Y. X. Wang, S. L. Chou, X. Ai, H. X. Yang, Y. L. Cao, *Angew. Chem. Int. Ed.* **2019**, *58*, 2.

[132] P. X. Xiong, X. P. Han, X. X. Zhao, P. X. Bai, Y. Liu, J. Sun, Y. H. Xu, *ACS Nano* **2019**, *13*, 2536.

[133] S. Gu, C. Sun, D. Xu, Y. Lu, J. Jin, Z. Wen, *Electrochem. Energy Rev.* **2018**, *1*, 599.

[134] L. Wang, Y. G. Wang, Y. Y. Xia, *Energy Environ. Sci.* **2015**, *8*, 1551.

[135] Y. Zhang, Y. Zhao, D. Gosselink, P. Chen, *Ionics* **2014**, *21*, 381.

[136] M. Nagao, Y. Imade, H. Narisawa, T. Kobayashi, R. Watanabe, T. Yokoi, T. Tatsumi, R. Kanno, *J. Power Sources* **2013**, *222*, 237.

[137] A. Hayashi, R. Ohtsubo, T. Ohtomo, F. Mizuno, M. Tatsumisago, *J. Power Sources* **2008**, *183*, 422.

[138] M. Nagao, A. Hayashi, M. Tatsumisago, *J. Mater. Chem.* **2012**, *22*, 10015.

[139] L. Zhan, Z. C. Liu, N. J. Dudney, C.D. Liang, *ACS Nano* **2013**, *7*, 2829.

[140] T. Tomonari, H. Kageyama, K. Nakanishi, M. Tabuchi, H. Sakaebe, T. Ohta, H. Senoh, T. Sakai, K. Tatsumi, *J. Electrochem. Soc.* **2010**, *157*, A1196.

[141] F. Han, J. Yue, X. Fan, T. Gao, C. Luo, Z. Ma, L. Suo, C. Wang, *Nano Lett.* **2016**, *16*, 4521.

[142] M. Eom, S. Son, C. Park, S. Noh, W. T. Nichols, D. Shin, *Electrochim. Acta* **2017**, *230*, 279.

[143] M. Shin, A. A. Gewirth, *Adv. Energy Mater.* **2019**, *9*, 1900938.

[144] R. Xu, J. Yue, S. Liu, J. Tu, F. Han, P. Liu, C. Wang, *ACS Energy Lett.* **2019**, *4*, 1073.

[145] Y. Zhang, R. Chen, T. Liu, B. Xu, X. Zhang, L. Li, Y. Lin, C. W. Nan, Y. Shen, *ACS Appl. Mater. Interfaces* **2018**, *10*, 10029.

[146] J. C. Bachman, S. Muy, A. Grimaud, H. H. Chang, N. Pour, S. F. Lux, O. Paschos, F. Maglia, S. Lupart, P. Lamp, L. Giordano, Y. Shao-Horn, *Chem. Rev.* **2016**, *116*, 140.

[147] R. Kanno, M. Murayama, *J. Electrochem. Soc.* **2001**, *148*, A742.

[148] T. Kobayashi, Y. Imade, D. Shishihara, K. Homma, M. Nagao, R. Watanabe, T. Yokoi, A. Yamada, R. Kanno, T. Tatsumi, *J. Power Sources* **2008**, *182*, 621.

[149] J. Yue, F. Han, X. Fan, X. Zhu, Z. Ma, J. Yang, C. Wang, *ACS Nano* **2017**, *11*, 4885.

[150] S. Goriparti, E. Miele, F. De Angelis, E. Di Fabrizio, R. Proietti Zaccaria, C. Capiglia, *J. Power Sources* **2014**, *257*, 421.

[151] A. R. Kamali, D. J. Fray, *J. New Mater. Electrochem. Syst.* **2010**, *13*, 147.

[152] L. Zhang, X. Liu, Q. Zhao, S. Dou, H. Liu, Y. Huang, X. Hu, *Energy Storage Mater.* **2016**, *4*, 92.

[153] Y. Yang, M. T. McDowell, A. Jackson, J. J. Cha, S. S. Hong, Y. Cui, *Nano Lett.* **2010**, *10*, 1486.

[154] A. R. Kamali, D. J. Fray, *Rev. Adv. Mater. Sci*. **2011**, *27*, 14.

[155] Y. Liang, W. H. Lai, Z. Miao, S. L. Chou, *Small* **2018**, *14*, 1702514.

[156] Z. X. Hao, J. Chen, L. X. Yuan, Q. M. Bing, J. H. Liu, W. L. Chen, Z. Li, F. R. Wang, Y. H. Huang, *Small* **2019**, *15*, 1902377.

[157] Y. Chen, S. T. Lu, Y. Li, W. Qin, X. H. Wu, *Mater. Lett.* **2019**, *248*, 157.

[158] S. Nanda, A. Gupta, A. Manthiram, *Adv. Energy Mater.* **2018**, *8*, 1801556.

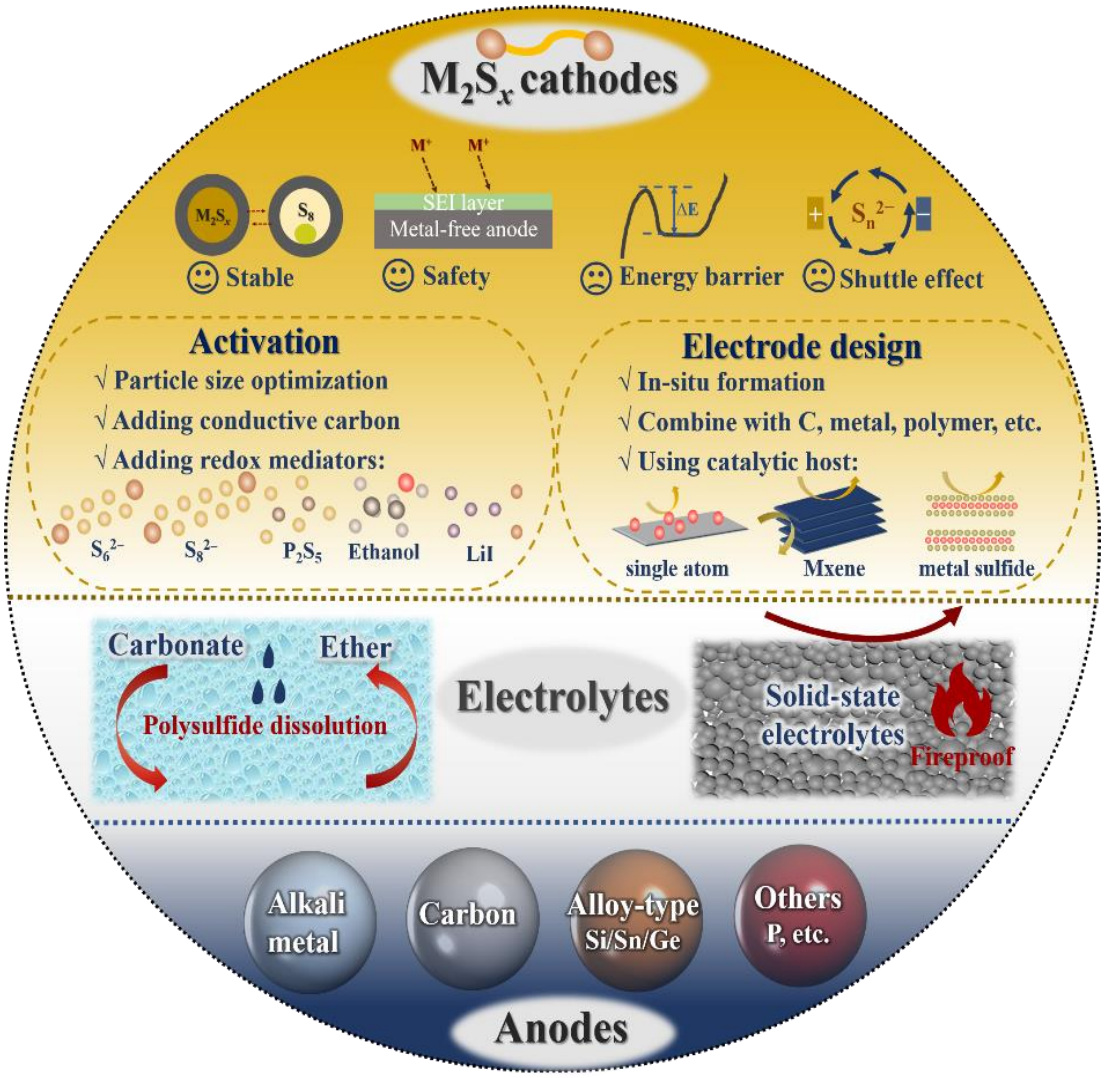

Figure 1. Schematic diagram of recapitulative study trends for M_2S_x cathode materials and M_2S_x cathode-based M–S batteries.

Table 1. Overview of the thermodynamically stable binary phases at room temperature for different metal–sulfur systems.

Phase diagram	Stale binary phases at RT	Ref.
Li–S	Li_2S	[34]
Na–S	Na_2S, Na_2S_2, Na_2S_4, Na_2S_5	[36,37]
K–S	K_2S, K_2S_2, K_2S_3, K_2S_4, K_2S_5, K_2S_6	[38]

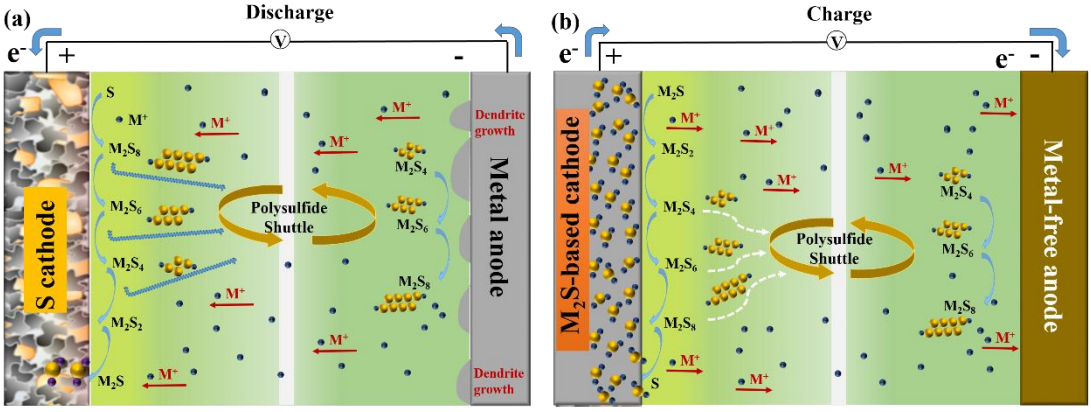

Figure 2. (a) Schematic diagram of M–S (M = Li, Na, K) batteries and (b) M_2S cathode-based M–S batteries with polysulfides present in the electrolyte, separately.

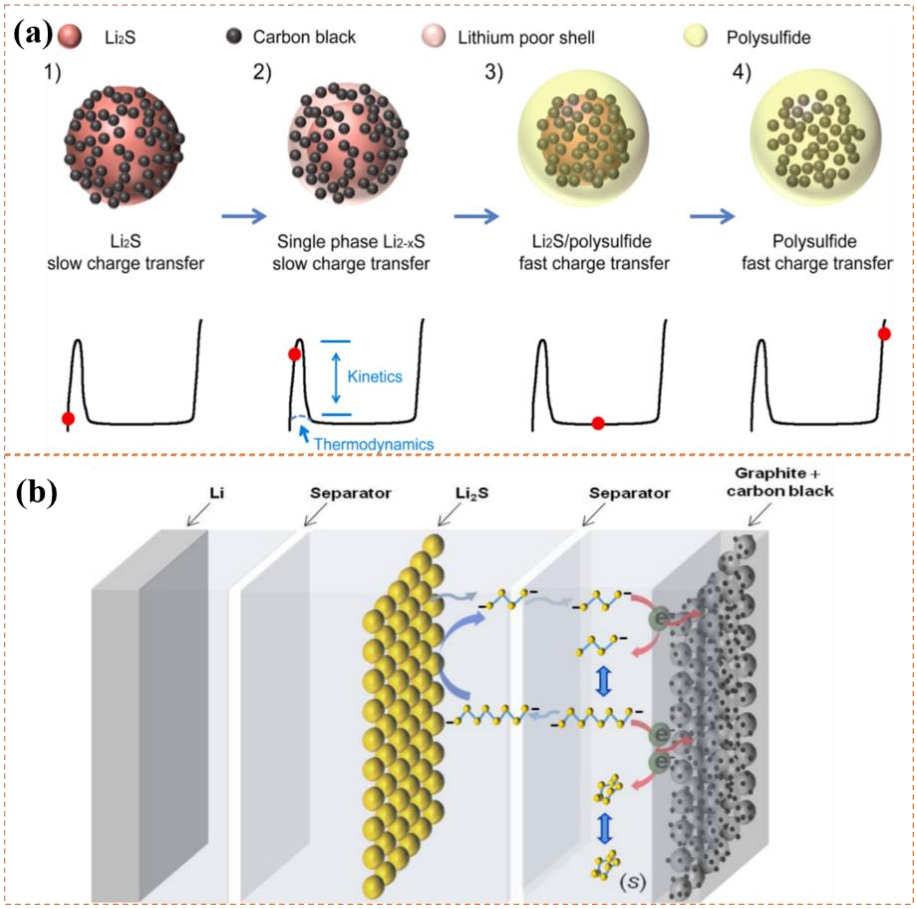

Figure 3. (a) Schematic illustrations of the first charging process in Li_2S cathode. Reproduced with permission.[20] Copyright 2012, American Chemical Society. (b) Schematic of a two-layer separator cell to detect possible oxidation route of solid Li_2S Particles. Reproduced with permission.[43] Copyright 2014, The Electrochemical Society.

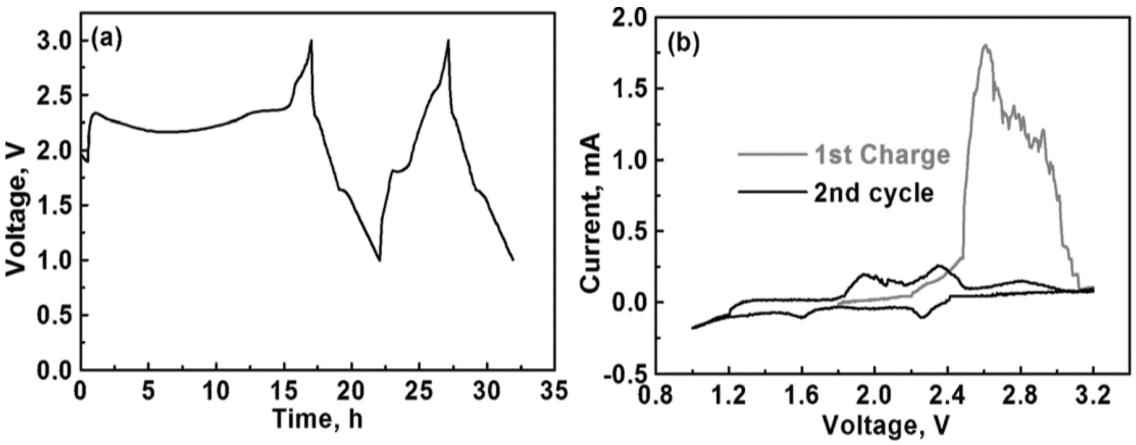

Figure 4. (a) Charge-discharge curves of the first two cycles of the Na_2S/multi-walled carbon nanotube (MWCNT) cathode-based RT Na–S battery. (b) Cyclic voltammograms of the Na_2S/MWCNT cathode-based half-cell at the scan rate of 0.1 mV s^{-1}. Reproduced with permission.[44] Copyright 2015, Wiley–VCH.

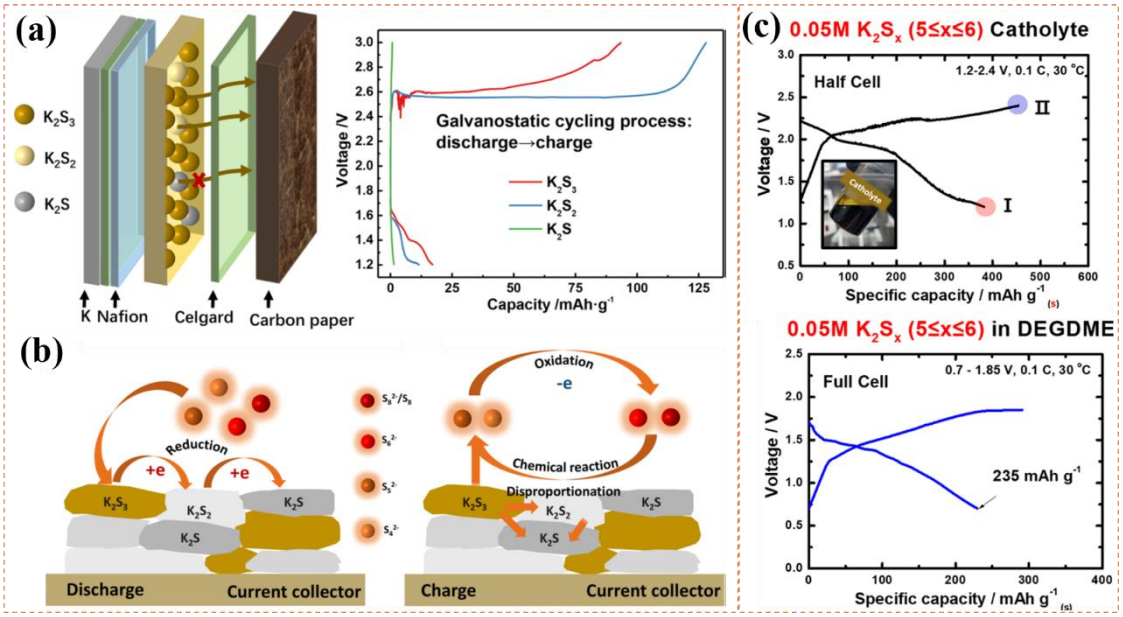

Figure 5. (a) Schematic diagram of the K_2S_x (x = 1, 2, and 3) battery double separators, with the cathode materials electrically isolated from the current collector, and charge-discharge curves of the batteries with different K_2S_x cathode, and (b) illustration of the mechanism of K_2S_x batteries during cycling: electrochemical reactions in discharging as well as the solution pathway reaction in charging. Reproduced with permission.[48] Copyright 2018, American Chemical Society. (c) Initial charge-discharge profiles of the K|K_2S_n catholyte|FCN half-cell, and the K impregnated HC|K_2S_n catholyte|FCN full-cell. Reproduced with permission.[49] Copyright 2018, American Chemical Society.

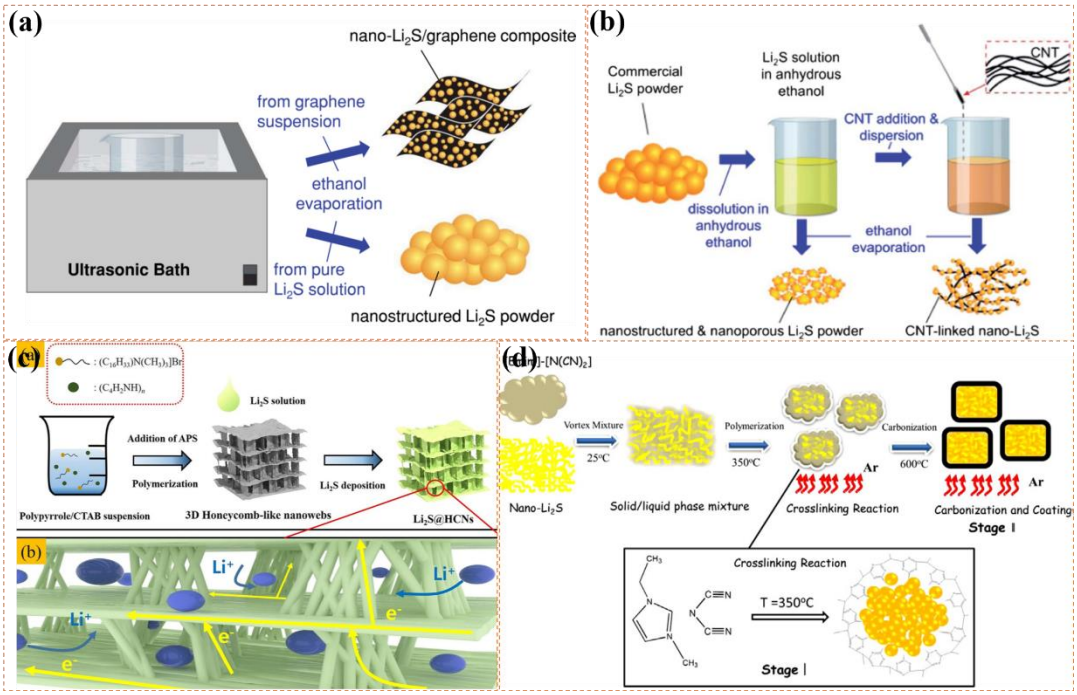

Figure 6. (a) Demonstration of the synthesis of Li_2S–graphene composite. Reproduced with permission.[61] Copyright 2014, Wiley–VCH. (b) Schematic illustration of the synthesis of nanostructured Li_2S and carbon nanotube (CNT)–Li_2S powder. Reproduced with permission.[62] Copyright 2014, Royal Society of Chemistry. (c) Schematic illustration of the synthesis of Li_2S@HCNs composites. Reproduced with permission.[63] Copyright 2019, Wiley–VCH. (d) Schematic illustration of the synthesis of carbon cage encapsulated Li_2S nano-cluster composite. Reproduced with permission.[64] Copyright 2015, ELSEVIER.

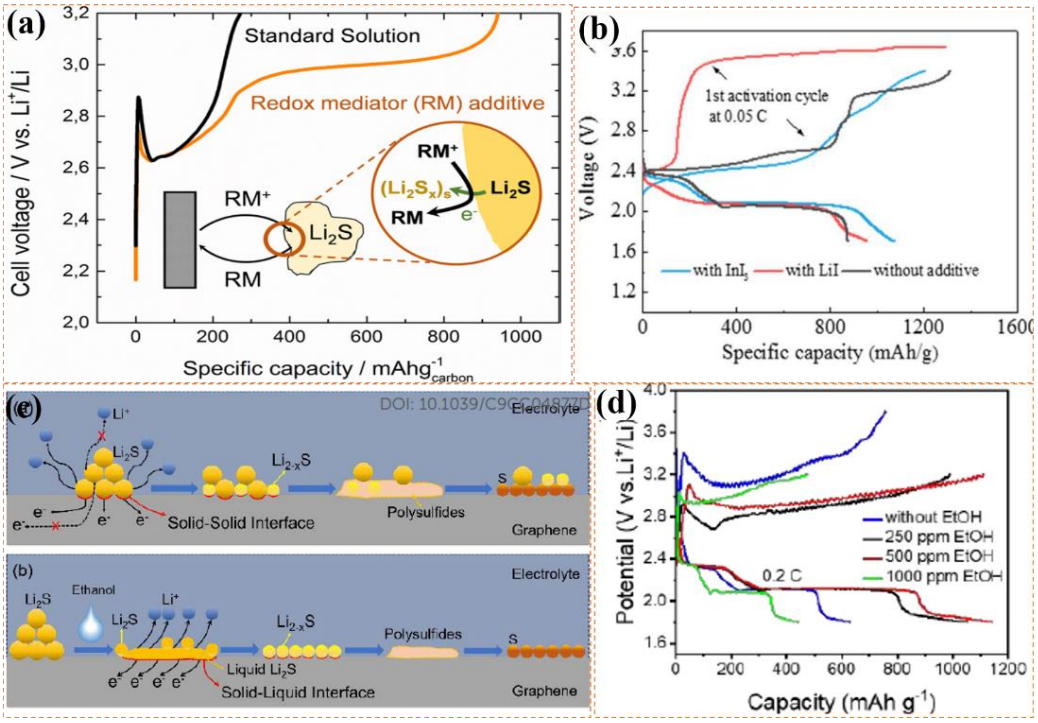

Figure 7. (a) Comparison of initial charge-discharge curves with/without redox mediator. Reproduced with permission.[22] Copyright 2014, American Chemical Society. (b) Comparison of the initial charge-discharge curves with/without InI_3. Reproduced with permission.[67] Copyright 2017, ELSEVIER. (c) Demonstration of the activation process of Li_2S without/with ethanol additive in the electrolyte, and (d) comparison of the initial charge-discharge curves with different amounts of ethanol. Reproduced with permission.[66] Copyright 2019, Royal Society of Chemistry.

Table 2 Comparison of the electrochemical performance of Li_2S cathodes formed via *in-situ* reactions.

Method	Li_2S content (wt %)	Electrolyte	Current collector	Loading (mg cm^{-2})	Initial/reversible discharge capacity (1^{st}/cycled, mA h g^{-1})	Rate performance	Ref.
Li_2SO_4 + Resorcinol-formaldehyde and CNT + calcination	~45	1 M LiTFSI in DOL/DME +2 wt% $LiNO_3$+0.01M Li_2S_6	Carbon paper	3	965 mA h g^{-1} at 0.05C/410 mA h g^{-1} after 200 cycles at 0.2C	555 mA h g^{-1} at 0.5C	[88]
				5	450 mA h g^{-1} after 200 cycles at 0.1C		
Li_2SO_4 + activated graphite+ calcination	68	1 M LiTFSI in DOL/DME +1 wt% $LiNO_3$	CNT film	0.48	500 mA h g^{-1} after 300 cycles at 0.5C	264.2 mA h g^{-1} at 4C	[80]
Li_2S_3+PVP+ calcination	72.2	1 M LiTFSI in DOL/DME +1 wt% $LiNO_3$	Al foil	1.5	~800 mA h g^{-1} at 0.025C/510 mA h g^{-1} after 100 cycles at 0.5C	170 mA h g^{-1} at 10C	[60]
$Li_2S{\cdot}H_2O$ + rGO + glucose + calcination	~40	1 M LiTFSI in DOL/DME +1 wt% $LiNO_3$	Al foil	0.8–1.0	819 mA h g^{-1} at 0.025C /469 mA h g^{-1} after 100 cycles at 0.1C	228 mA h g^{-1} at 2C	[81]
Li_2S_3+nitridated graphene+ calcination	~66.3	1 M LiTFSI in DOL/DME +1 wt% LiNO3+0.025M Li2S8	SACNT	~1.2	~950 mA h g^{-1} at 0.2C /480 mA h g^{-1} after 500 cycles at 0.2C	313 mA h g^{-1} at 2C	[89]
Li_2SO_4 + GO + Al_2O_3+ calcination	~58	1 M LiTFSI in DOL/DME +1 wt% $LiNO_3$	3 D graphene (free-standing)	1.2–1.5	866 mA h g^{-1} at 0.2C/736 mA h g^{-1} after 150 cycles at 0.2C/643 mA h g^{-1} after 300 cycles at 0.5C	546 mA h g^{-1} at 6C	[84]
Li_2SO_4 + PVA–CNT + calcination	40	1 M LiTFSI in DOL/DME +2 wt% $LiNO_3$	Free-standing	1.86	805 mA h g^{-1} at 0.1C/595 mA h g^{-1} after 150 cycles at 0.2C	496 mA h g^{-1} at 2C	[78]
Li_2SO_4 + FWNTs–GO + calcination	55–60	1 M LiTFSI in DOL/DME +1 wt% $LiNO_3$	Free-standing	1.0–1.5	980 mA h g^{-1} at 0.2C/868 mA h g^{-1} after 300 cycles at 0.2C	433 mA h g^{-1} at 10C	[83]
Li_2SO_4 + PVP + P–PANI + calcination	62	1 M LiTFSI in DOL/DME +1 wt% $LiNO_3$	nickel foam, filter paper, and carbon foam	2	1000 mA h g^{-1} at 0.1C/520 mA h g^{-1} after 100 cycles at 0.5C	530 mA h g^{-1} at 1C	[76]
				5	~370 mA h g^{-1} after 100 cycles at 0.5C		

Li_2SO_4 + PVP + calcination	50.6	1 M LiTFSI in DOL/DME +2 wt% $LiNO_3$	Free-standing	~3	~920 mA h g^{-1} at 0.1C/480 mA h after 200 cycles at 1C	460 mA h g^{-1} at 2C	[77]
Li_2SO_4 + CNT + sucrose + chitosan + calcination	60.2	1 M LiTFSI in DOL/DME +1 wt% $LiNO_3$	Al foil	~2	1014 mA h g^{-1} at 200 mA g^{-1} /671 mA h after 200 cycles at 200 mA g^{-1}	390 mA h g^{-1} at 3000 mA g^{-1}	[79]
Li_2SO_4 + chitosan + calcination	36	1 M LiTFSI in DOL/DME +1 wt% $LiNO_3$	Free-standing	~2	820 mA h g^{-1} at 0.1C/300 mA h after 100 cycles at 1C	180 mA h g^{-1} at 2C	[82]
S + $LiEt_3BH$ + chemical reaction	81–92	0.7 M LiTFSI in $PYR_{14}TFSI$/DME	Al foil	1.1–1.4	993 mA h g^{-1} at 0.2C/314 mA h g^{-1} after 1000 cycles at 2C	743 mA h g^{-1} at 2C	[86]
S + $LiEt_3BH$ + chemical reaction	88	1 M LiTFSI in $PYR_{14}TFSI$/DME+1 wt% $LiNO_3$	Carbon fiber paper	1.0–1.5	972 mA h g^{-1} at 0.5C/737 mA h g^{-1} after 100 cycles at 0.2C	793 mA h g^{-1} at 1C	[85]
S + $LiEt_3BH$ + chemical reaction	67	1 M LiTFSI in DOL/DME + 0.2 M $LiNO_3$+ 0.5 M polysulfides	Al foil	~1	1169 mA h g^{-1} at 0.05C/791 mA h g^{-1} after 100 cycles at 0.1C	565 mA h g^{-1} at 2C	[90]
Li + CS_2 + heat treatment	80	1 M LiTFSI in D2/DOL	Al foil	5	1120 mA h g^{-1} at 0.1C/702 mA h g^{-1} after 200 cycles at 160 mA g^{-1}	600 mA h g^{-1} at 2C	[86]
Li + CS_2 + heat treatment	38	Li7P3S11	-	~1.75	955 mA h g^{-1} at 0.2 mA cm^{-2}/1100mA h g^{-1} after 100 cycles at 0.2 mA cm^{-2}	800 mA h g^{-1} at 2 mA cm^{-2}	[91]
Li + MoS_2/rGO + electrochemical conversion	46.5	1 M LiPF6 in EC/DMC	Copper foam	4.3–5.1	956 mA h g^{-1} at 0.1C/606 mA h g^{-1} after 50 cycles at 0.1C	402 mA h g^{-1} at 2C	[92]

The discharge capacities are based on the mass of Li_2S.

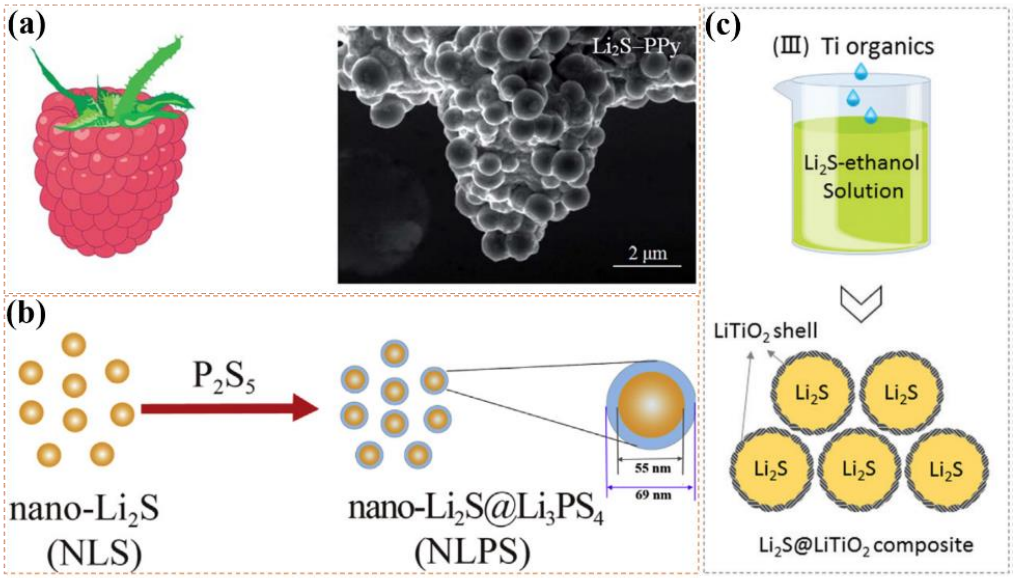

Figure 8. (a) Schematic illustration of a raspberry and the scanning electron microscope (SEM) image of a typical raspberry-like Li_2S–PPy composite. Reproduced with permission.[98] Copyright 2014, Royal Society of Chemistry. (b) Illustration of the synthesis process of the nano-Li_2S@Li_3PS_4 composite. Reproduced with permission.[99] Copyright 2017, ELSEVIER. (c) Schematic illustration of the scalable synthesis process for Li_2S@$LiTiO_2$ composite. Reproduced with permission.[68] Copyright 2018, Royal Society of Chemistry.

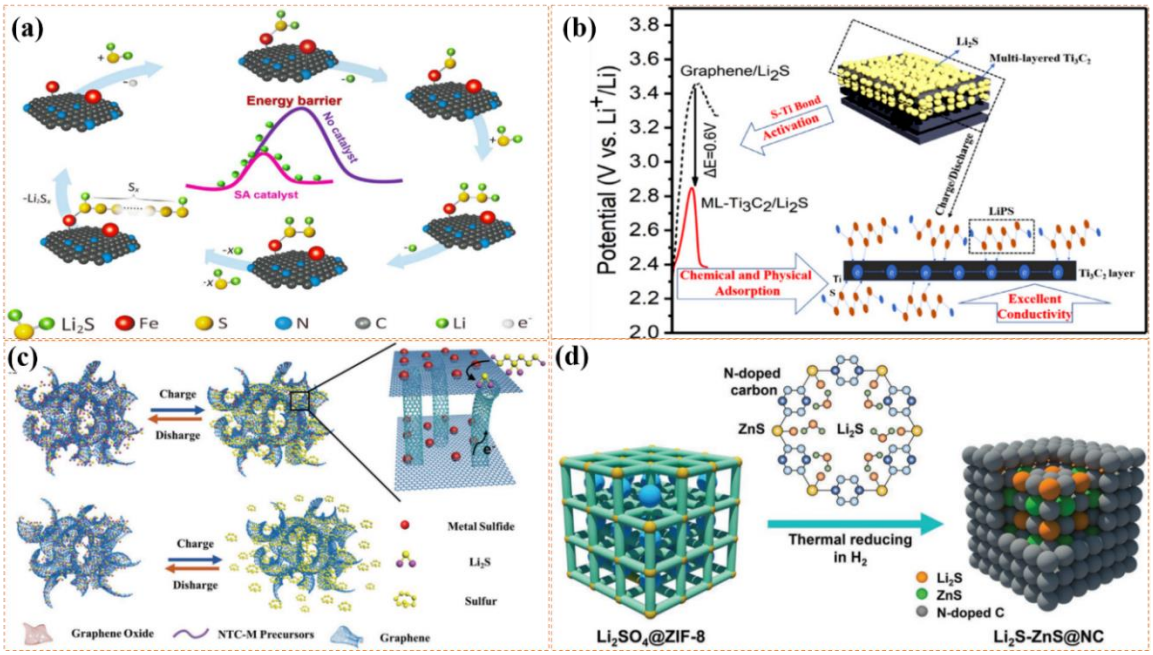

Figure 9. (a) Schematic illustration of SAFe catalyzed Li_2S delithiation reaction. Reprinted with permission.[108] Copyright 2018, ELSEVIER. (b) Schematic illustration of the structure and advantages of the ML–Ti_3C_2/Li_2S composite. Reprinted with permission.[112] Copyright 2019, ELSEVIER. (c) Schematic of the advantages of the 3DTSC composite. Reproduced with permission.[115] Copyright 2019, Wiley–VCH. (d) Schematic diagram of the synthesis of the Li_2S–ZnS@NC cathode. Reprinted with permission.[116] Copyright 2019, Wiley–VCH.

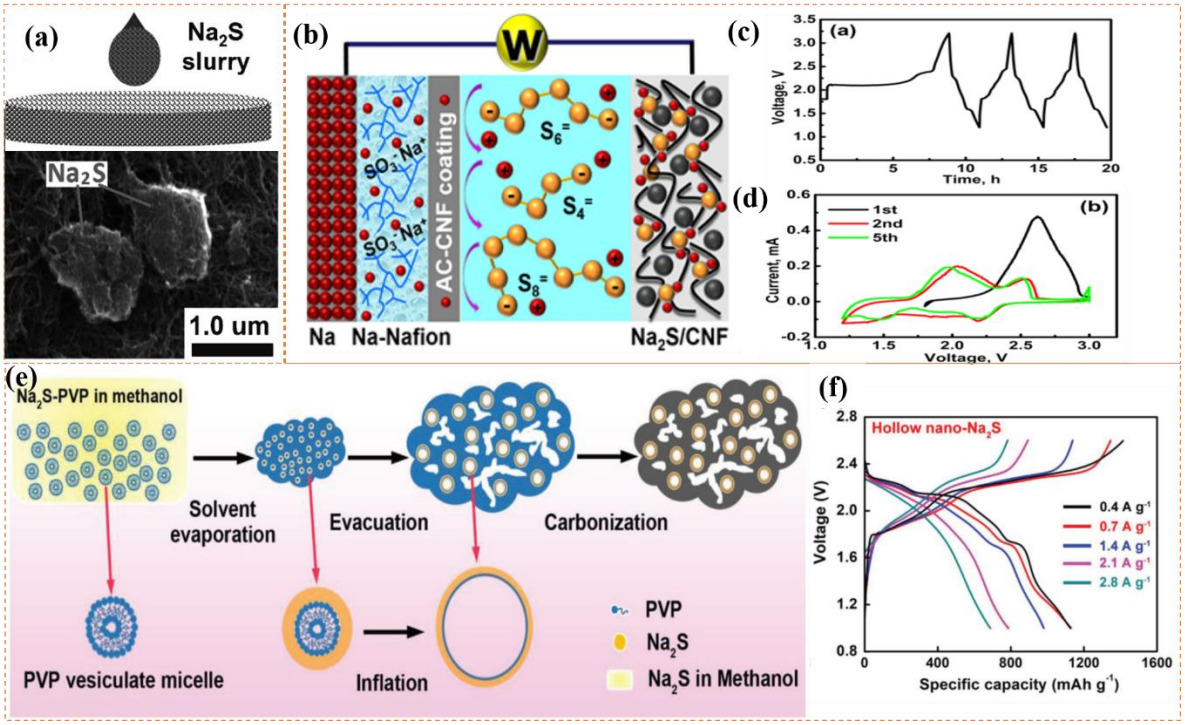

Figure 10. (a) Schematic illustration of the synthesis of a Na_2S/MWCNT electrode with Na_2S slurry, and an SEM image of the pristine Na_2S/MWCNT electrode. Reproduced with permission.[44] Copyright 2015, Wiley–VCH. (b) Schematic illustration of a Na‖Na-Nafion/CNF‖Na_2S/CNF cell, (c) Charge-discharge curves at 0.2 C and (d) cyclic voltammograms at 0.1 mV s^{-1} of Na‖Na-Nafion/ CNF‖Na_2S/CNF cell. Reproduced with permission.[121] Copyright 2016, American Chemical Society. (e) Schematic illustration of the synthesis of the hierarchical and spongy carbon-embedded hollow Na_2S nanosphere composite, and (f) charge-discharge curves of the hollow nano-Na_2S composite. Reproduced with permission.[123] Copyright 2018, Wiley–VCH.

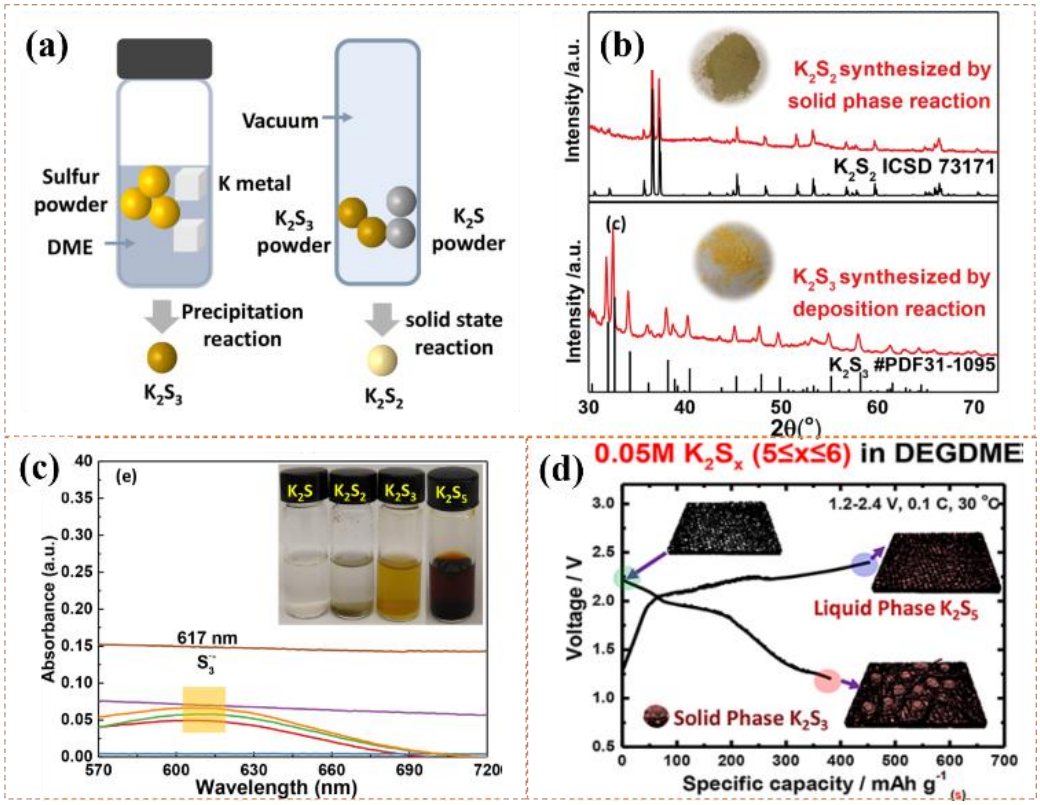

Figure 11. (a) Schematic illustration of the synthesis procedure for K_2S_2 and K_2S_3, (b) and (c) XRD and UV-vis spectra of the as-prepared K_2S_2 and K_2S_3 powders, with insert photographs. Reproduced with permission.[48] Copyright 2018, American Chemical Society. (d) First charge-discharge profiles of the K|K_2S_x catholyte|FCN half-cell in DEGDME. Reproduced with permission.[49] Copyright 2018, American Chemical Society.

Table 3 Comparison on the advantages and drawbacks for different types of electrolytes.

Electrolyte types	Ionic conductivity	Electrochemical stability	Thermal stability	Polysulfides dissolution	Interfacial stability	Safety
Carbonate	10^{-2}-10^{0} S cm^{-1}	limited to 4.5 V *vs* Li/Li^{+}	operate at room temperature	yes	stable SEI layer	flammable
Ether	10^{-2}-10^{0} S cm^{-1}	stable below 4.5 V *vs* Li/Li^{+}	operate at room temperature	yes	stable SEI layer	flammable
Solid state	10^{-4}-10^{-2} S cm^{-1}	stable up to 9 V *vs* Li/Li^{+}	stable up to 80ºC	no	high interfacial resistance	non-flammable

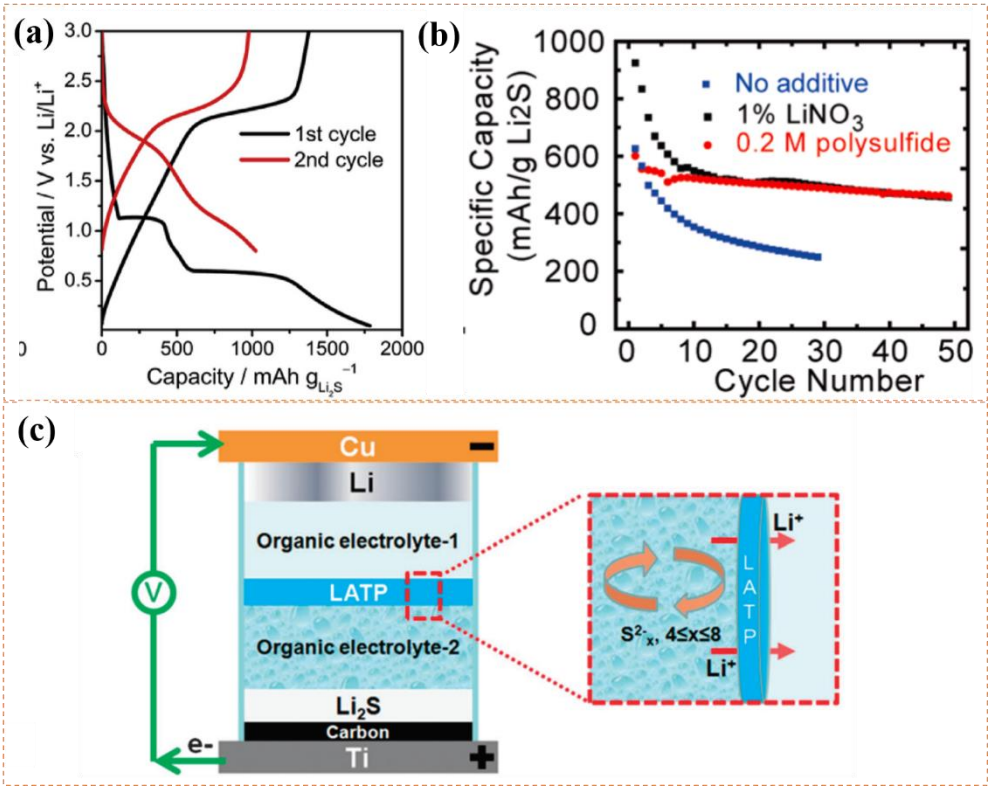

Figure 12. (a) Charge-discharge curves of 0.01 V ≤ *U* ≤ 3.0 V and 0.8 V ≤ *U* ≤ 3.0 V, where *U* is the potential, for the first two cycles of Li_2S cathodes in carbonate electrolyte. Reproduced with permission.[92] Copyright 2019, ELSEVIER. (b) The cycling performance of pristine Li_2S particles with different additives. Reproduced with permission.[20] Copyright 2012, American Chemical Society. (c) Schematic diagram of the architecture of a Li–S battery composed of (−) Cu/Li/electrolyte-1/separator/electrolyte-2/Li_2S cathode/carbon/Ti (+) from top to bottom. Reproduced with permission.[134] Copyright 2015, Royal Society of Chemistry.

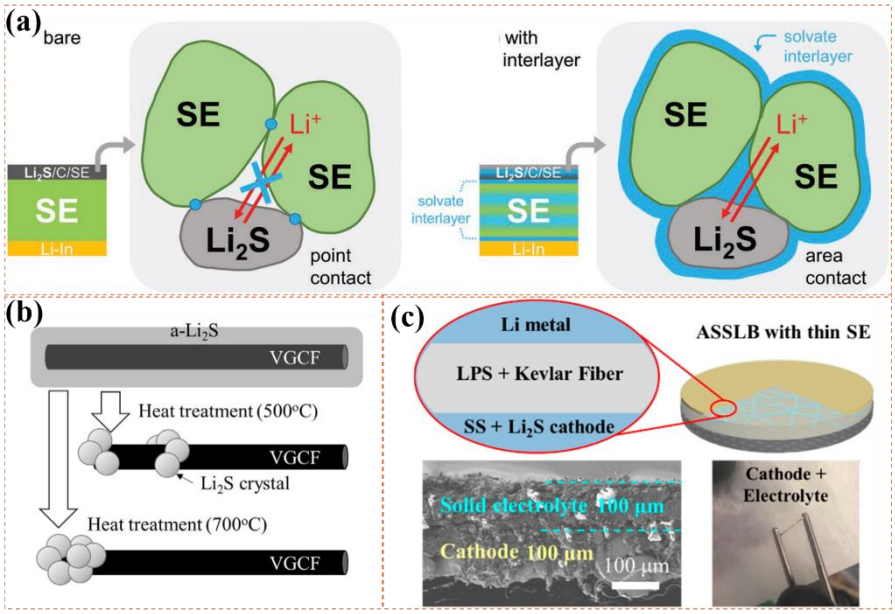

Figure 13. (a) Schematic illustration of the solid-state Li_2S batteries with Li–In alloy anode, LPS solid electrolyte, and Li_2S composite cathode. The composite cathode was prepared by ball-milling Li_2S, conductive carbon, and LPS. Reproduced with permission.[143] Copyright 2019, Wiley–VCH. (b) Schematic illustration of Li_2S–VGCF nanocomposite evolution versus temperature. Reproduced with permission.[142] Copyright 2017, ELSEVIER. (c) Schematic diagram of the cathode-supported all solid state cell with a thin Li_2S electrolyte. Reproduced with permission.[144] Copyright 2019, American Chemical Society.

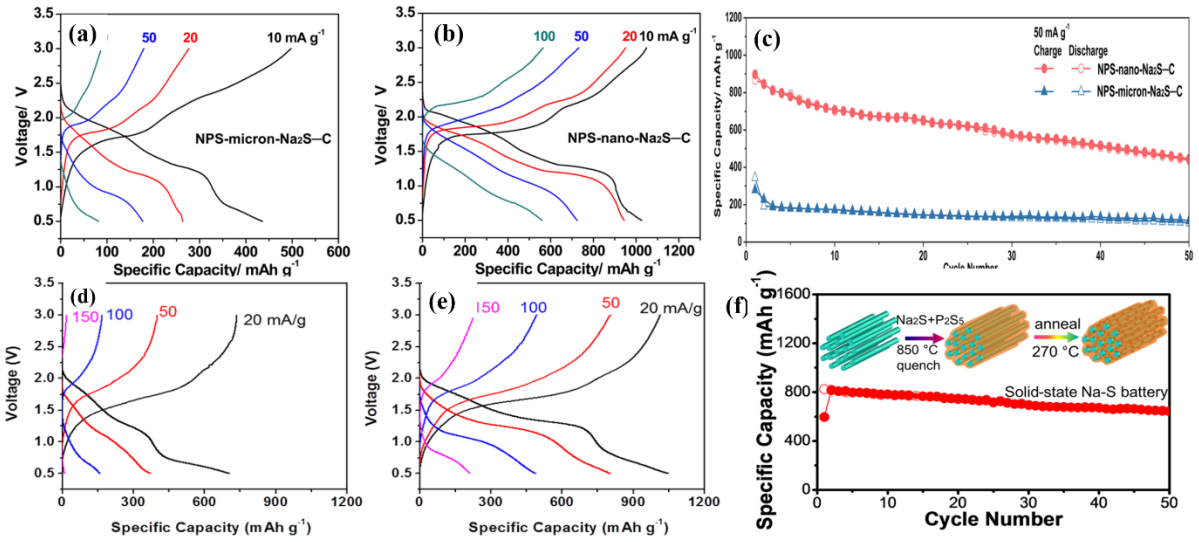

Figure 14. Charge-discharge curves of (a) the NPS-micro-Na_2S−C composite and (b) the NPS-nano-Na_2S−C composite cathodes in ASSBs at 60 °C, and (c) Cycling performance of the two Na_2S−C nanocomposite cathodes. Reproduced with permission.[149] Copyright 2017, American Chemical Society. (d) Charge-discharge curves of the ball-milled Na_2S−C composite and (e) cast-annealed Na_2S−C composite cathodes in ASSBs at 60 °C, and (f) Cycling performance of the solid-state Na–S battery. Reproduced with permission.[54] Copyright 2018, American Chemical Society.

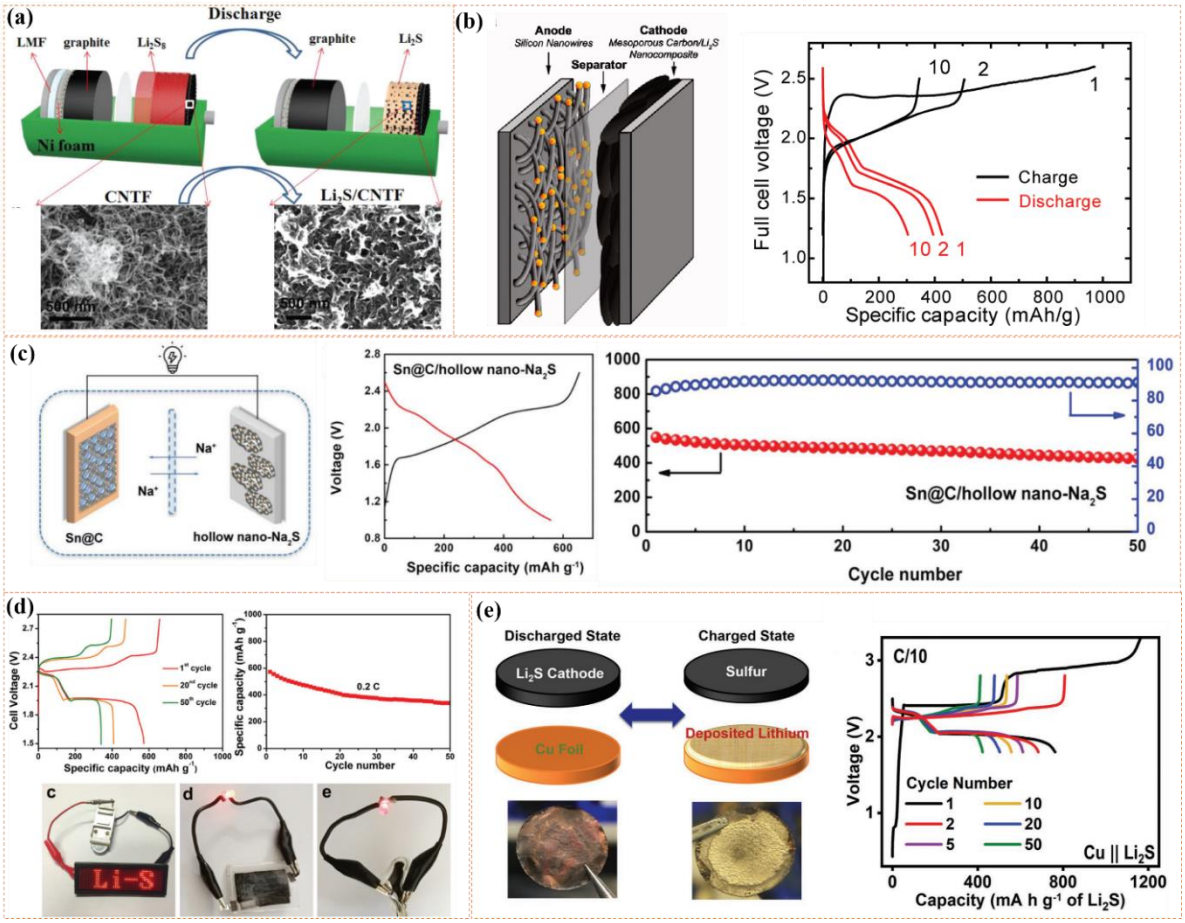

Figure 15. (a) Schematic illustration and SEM images of the synthesis procedure for *in-situ* electrochemical conversion in a Li_2S/graphite full-cell. Reproduced with permission.[93] Copyright 2018, Wiley–VCH. (b) Schematic diagram of the structure of a Li_2S/Si full-cell and the corresponding charge-discharge profiles. Reproduced with permission.[153] Copyright 2010, American Chemical Society. (c) Schematic diagram of the configuration of a non-Na metal Sn@C||Na_2S full-cell and its corresponding electrochemical performance. Reproduced with permission.[118] Copyright 2018, Wiley–VCH. (d) Typical discharge-charge voltage profiles and cycling performance of the Li_2S@CNF||Fe_3O_4 full-cell at 0.2 C between 1.5 − 2.8 V. Reproduced with permission.[50] Copyright 2017, Wiley–VCH. (e) Schematic illustration photographs of the Cu || Li_2S full-cell and corresponding charge-discharge curves. Reproduced with permission.[158] Copyright 2018, Wiley–VCH.

Table 4. Research on the metal-free anodes for alkali-metal sulfide based metal–sulfur batteries.

Anode	Electrolyte	Cathode	Voltage (V *vs.* Li/Li^+)	Capacity/ mA h g^{-1}	Specific energy density	Cycling ability	Ref.
Graphite	1 M LiTFSI in DOL/DME +1 wt% $LiNO_3$	Li_2S	1.3–2.8	initial capacity of 1006 mA h g^{-1} at 0.2C	-	378 mA h g^{-1} after 500 cycles at 0.2C	[93]
Graphite	2.4 M LiTFSI in DOL/DME +0.24 M LiI	Li_2S@$LiTiO_2$	1.0–2.8	initial capacity of 1089 mA h g^{-1} at 0.2C	-	718 mA h g^{-1} (71%)after 150 cycles at 0.5C	[68]
Hard carbon	1 M $NaClO_4$ in TEGDME	Na_2S/C	0.2–2.5	initial capacity of 297 mA h g_s^{-1}	-	stable cycling over 10 cycles	[130]
Hard carbon	0.5 M KTFSI in DEGDME	K_2S_x($5\leq x \leq 6$)	0.7–1.85	initial capacity of 235 mA h g^{-1} at 0.1C	-	-	[49]
Si	1 M LiTFSI in DOL/DME	Li_2S/CMK-3	1.2–2.6	Initial discharge 423 mA h g^{-1} at C/3	Initial 630 W h kg^{-1}	>200 mA h g^{-1} over 20 cycles at C/3	[153]
Si	1 M LiTFSI in DOL/DME +2 wt% $LiNO_3$	Li_2S@C	1.7–2.8	initial capacity of 470 mA h g_{Li2S}^{-1} at 0.1C	-	-	[88]
Si	1 M LiTFSI in DOL/DME +2 wt% $LiNO_3$	Li_2S–ZnS@NC	1.2–2.5	initial capacity of 710 mA h g^{-1} at 0.2C	673 W h kg^{-1}	57.7% capacity retention for 200 cycles at 0.2C	[116]
Si	1 M LiTFSI in DOL/DME +2 wt% $LiNO_3$	TiN/PHC@Li_2S	1.3–2.8	initial capacity of 702 mA h g_{Li2S}^{-1} at 0.5C	252 W h kg^{-1}	0.4% capacity fade per cycle over 200 cycles at 0.5C	[156]
Sn@C	1 M $NaPF_6$ in DEGDME/ DOL	Hollow nano-Na_2S/C	1.0–2.6	initial capacity of 550 mA h g_s^{-1} at 0.7 A g^{-1}	-	80% capacity retention for 50 cycles at 0.7 A g^{-1}	[123]
SnO_2	1 M LiTFSI in DOL/DME +1 wt% $LiNO_3$	Li_2S	0.8-2.8	Initial discharge ~750 mA h g^{-1} at 0.5C	~352 W h kg^{-1}	~647 mA h g^{-1} over 200 cycles at 0.5C	[33]
P/C	1 M LiTFSI in DOL/DME	Li_2S	0-2.8	Second cycle capacity of 550 mA h g^{-1} at 0.2C	-	378 mA h g^{-1} over 200 cycles at 0.5C	[18]
Fe_3O_4	1 M LiTFSI in DOL/DME +2 wt% $LiNO_3$	Li_2S/NC NF paper	1.5–2.8	initial capacity of 576 mA h g^{-1} at 0.2C	403 W h kg^{-1}	60% capacity retention for 50 cycles at 0.2C	[77]

MnO_2-rGO	1 M LiTFSI in DOL/DME	Li_2S-rGO	0.2–2.6	initial capacity of 587 mA h g_{Li2S}^{-1} at 0.2C	827 W h kg_{Li2S}^{-1}/ 455 Wh $kg_{Cathode}^{-1}$	80.5% capacity retention for 150 cycles at 0.2C	[157]
Cu	-	Li_2S	1.8–2.8	initial capacity of 919 mA h g^{-1} at 0.1C	-	70% capacity retention for 100 cycles at 0.1C	[158]

The discharge capacities and specific energy are based on the active material mass on both electrodes unless otherwise stated.